Measurement report: The Fifth International Workshop on Ice Nucleation Phase 1 (FIN-01): Intercomparison of Single Particle Mass Spectrometers

Xiaoli Shen[1], David M. Bell[2,a], Hugh Coe[3,4], Naruki Hiranuma[5,b], Fabian Mahrt[6,c], Nicholas A. Marsden[3,4], Claudia Mohr[5,a,d], Daniel M. Murphy[7], Harald Saathoff[5], Johannes Schneider[8], Jacqueline Wilson[2,e], Maria A. Zawadowicz[9,f], Alla Zelenyuk[2], Paul J. DeMott[10], Ottmar Möhler[5], and Daniel J. Cziczo[1,9,11]

[1]Department of Earth, Atmospheric, and Planetary Sciences, Purdue University, West Lafayette, IN 47907, USA
[2]Atmospheric, Climate, and Earth Sciences Division, Pacific Northwest National Laboratory, Richland, WA 99354, USA
[3]Department of Earth and Environmental Sciences, University of Manchester, Manchester, M13 9PL, UK
[4]National Centre for Atmospheric Sciences, University of Manchester, Manchester, M13 0PL, UK
[5]Institute of Meteorology and Climate Research, Karlsruhe Institute of Technology, Eggenstein-Leopoldshafen, 76344, Germany
[6]Department of Environmental System Sciences, Institute for Atmospheric and Climate Science, ETH Zürich, Zurich, 8092, Switzerland
[7]Earth System Research Laboratory, National Oceanic and Atmospheric Administration, Boulder, CO 80305, USA
[8]Max Planck Institute for Chemistry, Mainz, 55128, Germany
[9]Department of Earth, Atmospheric, and Planetary Sciences, Massachusetts Institute of Technology, Cambridge, MA 02139, USA
[10]Department of Atmospheric Science, Colorado State University, Fort Collins, CO 80523-1371, USA
[11]Department of Civil and Environmental Engineering, Massachusetts Institute of Technology, Cambridge, MA 02139, USA
[a]now at: Laboratory of Atmospheric Chemistry, Paul Scherrer Institute, 5232 Villigen, Switzerland
[b]now at: Department of Life, Earth, and Environmental Sciences, West Texas A&M University, Canyon, TX 79016, USA
[c]now at: Department of Chemistry, Aarhus University, DK-8000 Aarhus, Denmark
[d]now at: Department of Environmental Systems Science, ETH Zürich, 8092 Zürich, Switzerland
[e]now at: UK Health Security Agency, Oak Park Lane, Cookridge, Leeds, West Yorkshire LS16 6RW, UK
[f]now at: Environmental and Climate Sciences Department, Brookhaven National Laboratory, Upton, NY 11973, USA

Correspondence to: Xiaoli Shen (xlshen@purdue.edu)

Abstract. Knowledge of chemical composition and mixing state of aerosols at a single particle level is critical for gaining insights into atmospheric processes. One common tool to make these measurements is single particle mass spectrometry. There remains a need to compare the performance of different single particle mass spectrometers (SPMSs). An intercomparison of SPMSs was conducted at the Aerosol Interaction and Dynamics in the Atmosphere (AIDA) chamber at the Karlsruhe Institute of Technology (KIT) in November 2014, as the first phase of the Fifth International Workshop on Ice Nucleation (FIN-01). In this paper we compare size distributions and mass spectra of atmospherically relevant particle types measured by five SPMSs. These include different minerals, desert and soil dusts, soot, bioaerosol (Snomax; protein granule), secondary organic aerosol (SOA) and SOA coated mineral particles. All Most SPMSs reported similar vacuum aerodynamic diameter (d_{va}) within typical instrumental ranges from ~100–200 nm (lower limit) to ~2–3 μm (upper limit). In general, all SPMSs exhibited a wide dynamic

range (up to ~10^3) and high signal to noise ratio (up to ~10^4) in mass spectra. Common spectral features with small diversities in mass spectra were found with high average Pearson's correlation coefficients, i.e., for average positive spectra $r_{avg-pos} = 0.74 \pm 0.12$ and average negative spectra $r_{avg-neg} = 0.67 \pm 0.22$. ~~The highest correlation of average mass spectra across all instruments was observed for Snomax ($r_{avg-pos} = 0.92 \pm 0.04$ and $r_{avg-neg} = 0.90 \pm 0.05$), attributed to the prevalence of common markers and similar spectral patterns. The poorest correlation was found for propane soot ($r_{avg-pos} = 0.51 \pm 0.23$ and $r_{avg-neg} = 0.35 \pm 0.26$), primarily because of low detection efficiency (DE) due to small particle size.~~ We found that instrument-specific DE was more dependent on particle size than particle type~~. We also found that~~, and particle identification favored the use of bipolar, rather than monopolar, instruments. Particle classification from "blind experiments" showed that all instruments differentiated SOA, soot, and soil dust, and detected subtle changes in the particle internal mixing, but had difficulties differentiating among specific mineral types and dusts. This study helps to further understand the capabilities and limitations of the single particle mass spectrometry technique in general, as well as the specific instrument performance in characterizing atmospheric aerosol particles. ~~We propose that intercomparison workshops should continue as new SPMSs are developed and, ideally, should include both laboratory and field activities.~~

1 Introduction

Aerosol-cloud interactions are one of the largest uncertainties in the climate system (IPCC, 2021). A considerable source of uncertainty is related to an insufficient understanding of how chemical composition of aerosols affects their ability to act as cloud condensation nuclei (CCN) and ice nucleating particles (INPs). Both CCN and INPs influence cloud formation, microphysical and radiative properties, and precipitation formation and hence impact climate and the hydrological cycle (Lohmann et al., 2016). Studying INPs is particularly challenging, given that in the atmosphere only ~1 in ~10^5 particles act as an INP (Rogers et al., 1998). The low number concentration of INPs and the complex atmospheric aging processes that can affect the particle's ability to nucleate ice, including the acquisition of coatings and/or evaporation of components (Cziczo et al., 2009; Friedman et al., 2011; Möhler et al., 2008), can challenge current measurement techniques (Cziczo et al., 2003, 2017; Fuzzi et al., 2015; Kanji et al., 2017). Knowledge of chemical composition and mixing state on a single particle level is therefore critical to understand atmospheric processes and correctly predicting atmospheric impacts (Riemer et al., 2019).

In the past three decades in-situ and real-time single particle mass spectrometry has been widely used to characterize the size and composition of individual particles (Murphy, 2007). Corresponding studies have led to an improved understanding of internal and external mixing of ambient aerosol particles, as well as particle origin and chemical transformation (Noble and Prather, 2000; Pratt and Prather, 2012). The first airborne single particle chemical characterization of cirrus ice residues (IRs, the particle remaining after ice crystal sublimation) was in the 2001 CRYSTAL-FACE study (Cziczo et al., 2004). Since then, the single particle mass spectrometer (SPMS) has emerged as the powerful tool for assessing the chemical composition of ice-nucleating particles (INPs) and for direct measurements of IRs (Cornwell et al., 2019; Cziczo et al., 2003, 2006, 2009, 2013, 2017; Cziczo and Froyd, 2014; DeMott et al., 2003; Kamphus et al., 2010; Lacher et al., 2021; Lin et al., 2017; Pratt and

70 Prather, 2009; Roth et al., 2016; Sullivan et al., 2010). This was one of the major motivating factors for organizing the intercomparison of SPMSs within the framework of the Fifth International Ice Nucleation (FIN) Workshops, which sought to conduct comprehensive comparisons of instruments in both laboratory and field settings. Further information about the FIN workshops can be found in DeMott et al. (2011, 2018). The first phase (FIN-01), focused on intercomparing SPMSs, was conducted at the Aerosol Interaction and Dynamics in the Atmosphere (AIDA) chamber located at the Karlsruhe Institute of

75 Technology (KIT) in November 2014.

Since their inception, SPMS design has varied from instrument to instrument while also continuously undergoing improvements (Brands et al., 2011; Clemen et al., 2020; Cziczo et al., 2006; Dragoneas et al., 2022; Du et al., 2024; Erdmann et al., 2005; Gaie-Levrel et al., 2012; Gemayel et al., 2016; Hünig et al., 2022; Jacquot et al., 2024; Li et al., 2011; Marsden et al., 2016; Passig et al., 2020; Prather et al., 1994; Thomson et al., 2000; Trimborn et al., 2000; Zawadowicz et al., 2020;

80 Zelenyuk et al., 2009b, 2015; Zelenyuk and Imre, 2005). Unlike the Aerodyne Aerosol Mass Spectrometer (AMS), used for bulk measurements of non-refractory aerosol components (DeCarlo et al., 2006), no commercial instrument has dominated SPMS design. Design choices and technical details were reviewed by Murphy (2007). SPMSs have various characteristics, some of which are instrument specific, but instruments have some similar components, including an inlet system, a particle detection and sizing region, an ionization region, and one or two mass spectrometers. Here, we will briefly describe some of

85 these key features:

1) A critical orifice, capillary, or aerodynamic lens (ADL) inlet to transmit and focus particles into a narrow beam in a low pressure region (Davis, 1977; Liu et al., 1995; Murphy and Thomson, 1995).

2) A detection and sizing region using one or two continuous wave (CW) lasers, e.g., 532 nm Neodymium-doped Yttrium Aluminum Garnet (Nd:YAG) or 405 nm laser diodes. In this region, particle light scattering and the vacuum aerodynamic

90 diameter (d_{va}) of individual particles are determined and recorded. Particles with d_{va} from ~100 nm up to ~3 μm are generally detected. Detection is influenced by several factors, such as the particle size, shape, morphology, and optical properties of particles, the wavelength, power, and beam dimensions of the detection lasers, as well as the distance between two lasers (Gemayel et al., 2016; Sinha and Friedlander, 1985; Su et al., 2004).

3) An ion source region where one or two laser pulses provides laser desorption and ionization (LDI). This allows for

95 subsequent identification of most particulate components from volatile and semi-volatile to refractory. For one step LDI, a pulsed UV laser, e.g. 193 nm Argon Fluoride (ArF) excimer or 266 nm Nd:YAG laser, is triggered to ablate and ionize the particle after detection (McKeown et al., 1991; Prather et al., 1994). Two-step LDI often employs an infrared (IR) pulse (e.g., CO_2 laser) for desorption followed by a lower wavelength pulse for ionization (Cabalo et al., 2000; Zelenyuk et al., 1999, 2009b). Two-step LDI is commonly used to reduce ion fragmentation (Morrical et al., 1998; Zelenyuk et al., 2009a). In

100 addition, as part of the ionization occurs in the particle's gaseous plume, quantification can be improved (Woods et al., 2001) and resonance effects can be used to increase the sensitivity to organics (Passig et al., 2022; Schade et al., 2019).

4) One or two mass spectrometers, most commonly time-of-flight (ToF), are used for measurement of ions (Gard et al., 1997; Murphy and Thomson, 1995).

There are limitations inherent to laser ablation and ionization of atmospheric particles with respect to reproducibility of mass

105   spectra and quantitative assessment of single particle composition. The complexity of LDI mechanisms varies between instruments due to ionization laser wavelength and laser power intensity at the point of ablation/ionization. Different SPMSs may have differences in completeness of particle ablation, leading to diversity in spectral signatures (Murphy, 2007; Reilly et al., 2000; Reinard and Johnston, 2008; Thomson et al., 1997; Zenobi and Knochenmuss, 1998). Effort has been put in to refining particle identification but quantification of specific particle components remains a challenge (Allen et al., 2006, 2000;

110   Bein et al., 2006; Fergenson et al., 2001; Froyd et al., 2019; Gallavardin et al., 2008; Gemayel et al., 2017; Gross et al., 2000; Gunsch et al., 2018; Hatch et al., 2014; Healy et al., 2013; Jeong et al., 2011; Köllner et al., 2017; Lu et al., 2018; Marsden et al., 2018, 2019; May et al., 2018; Qin et al., 2006; Ramisetty et al., 2018; Shen et al., 2018, 2019; Wenzel et al., 2003; Zawadowicz et al., 2017, 2020; Zhou et al., 2016). Data analysis and classification methods used by different SPMSs can also differ substantially.

115   Intercomparisons of SPMSs and data analysis methods remain rare (Kamphus et al., 2010; Lacher et al., 2021; Middlebrook et al., 2003; Murphy et al., 2007). Middlebrook et al. (2003) reported a comparison of SPMSs, including the Particle Analysis by Laser Mass Spectrometer (PALMS, National Oceanic and Atmospheric Administration, NOAA), Aerosol Time-of-Flight Mass Spectrometer (ATOFMS, University of California at Riverside), and Rapid Single-Particle Mass Spectrometer II (RSMS-II, University of Delaware) during the Atlanta Supersite Project in 1999. They found comparable particle classes with similar

120   number fractions measured by the three SPMSs for the entire measurement period. Murphy et al. (2007) showed geographically broad distribution of lead in single particles, by comparing and combing the results from aircraft and ground-based measurements of different SPMSs: PALMS, a commercial ATOFMS (Model 3800, TSI, USA), and RSMS. Kamphus et al. (2010) compared the Single Particle Laser-Ablation Time-of-Flight Mass Spectrometer (SPLAT, Max Planck Institute for Chemistry, MPIC) and a commercial ATOFMS at the Jungfraujoch research station and showed comparable results for IRs

125   and droplet residuals. They also reported differences due to different ionization lasers and detection efficiencies for the two instruments. In a similar study, Lacher et al. (2021) showed comparable results of total aerosol composition from the Aircraft-based Laser ABlation Aerosol MAss Spectrometer (ALABAMA, MPIC) and the Laser Ablation Aerosol Time-of-Flight Mass Spectrometer (LAAPTOF, AeroMegt GmbH, Germany) for ambient measurements at the Jungfraujoch.

One of the main goals of FIN-01 was to intercompare some of the major SPMSs used for atmospheric aerosol research. This

130   included the custom-built instruments PALMS (Massachusetts Institute of Technology, MIT) (Cziczo et al., 2006), ALABAMA (MPIC) (Brands et al., 2011), and miniSPLAT (Pacific Northwest National Laboratory, PNNL) (Zelenyuk et al., 2015) and the commercial instruments ATOFMS (TSI Model 3800, USA; from the Eidgenössische Technische Hochschule, ETH) (Gard et al., 1997; Prather et al., 1994) and LAAPTOF (AeroMegt GmbH, Germany; from University of Manchester, UoM) (Marsden et al., 2016).

135   The specific objectives of FIN-01 were:

1) Compare mass spectral signatures for key atmospheric particle types, including desert and soil dusts, soot and biological particles, as well as particles with coatings.

2) Compare instrument performance and data analysis techniques in "blind experiments", where participants did not know the particle types being sampled.

3) Evaluation of the SPMSs' ability to measure the chemical composition of IRs.

This paper provides an overview of FIN-01. Experiments on particles with coatings by organics are discussed in more details elsewhere (Bertozzi, 2022; Bertozzi et al., 2024).

2 Methods

More than ninety independent experiments were conducted during the FIN-01 workshop. Nine co-located SPMSs and ancillary aerosol characterization instrumentation were utilized. Here we focus on a subset, fourteen specific experiments, targeting the objectives listed above. Data were provided for five of the nine SPMSs deployed during FIN-01: ALABAMA, miniSPLAT, PALMS and a commercial ATOFMS and LAAPTOF.

2.1 SPMSs

Table 1 summarizes the main components and performance parameters of the five SPMSs. Note that the values summarized in Table 1 and presented in this section are attributions to the current literature and were not independently verified during FIN-01. All instruments have been described in detail previously (Brands et al., 2011; Cziczo et al., 2006; Gard et al., 1997; Gemayel et al., 2016; Marsden et al., 2016; Prather et al., 1994; Shen et al., 2018; Su et al., 2004; Zelenyuk et al., 2015). They are functionally similar, but some instrumental differences are noteworthy: All used an ADL, but not with the same inlet flowrate. Laser wavelength, laser power, focal spot size, and beam direction varied across the instruments. Laser differences can impact several measurement parameters:

1) Detectable particle size range. PALMS, LAAPTOF, and ATOFMS detected similar size range of ~100-200 nm to ~3 μm d_{va}, ALABAMA detected a narrower range of ~200 nm to ~1 μm d_{va}, while miniSPLAT detected ~50 nm to ~1.4 μm d_m (electrical mobility diameter).

2) Detection efficiency (DE) is defined as the ratio of the number of particles detected and/or sized to the total number of particles entering the inlet. All instruments exhibited size dependent-DE for spherical polystyrene latex (PSL) particles. Most instruments also exhibit a less pronounced size dependence on morphology. It is important to note that DE for miniSPLAT has been defined differently from the other SPMSs. MiniSPLAT operates simultaneously in a "dual data acquisition mode" where the size distribution is determined at a rate up to several thousand particles per second, while single particle mass spectra, and corresponding d_{va}, are acquired at a rate similar to the other SPMSs, ~20 particles per second (Zelenyuk et al., 2015). For particle size measurements, miniSPLAT often uses a dilution stage to lower aerosol number density to reduce coincidence of multiple particles in the detection laser beams. The variable amount of dilution for FIN-01 was not reported and is therefore not addressed in this paper. The DE of miniSPLAT, for comparison to the other instruments, can be referenced either to the ratio of total particles sized after the dilution stage or the ratio of the particles for which the laser was triggered. The former is

a more direct comparison of DE to the other SPMSs, but both are presented here for clarity. Note that the other SPMSs run in a single acquisition mode which records single particle mass spectra and corresponding sizes. Most often, particles size distributions are acquired by separate instruments running in parallel. This difference in methodology leads to differences in terminology, which are described here when relevant.

3) Hit rate (HR) is most commonly defined as the ratio of the number of useful spectra generated to the number of detected particles. PALMS had a HR of ~95% without obvious size or shape dependency (Cziczo et al., 2006), largely due to the proximity of the final detection beam and the ablation and ionization location. Other instruments had larger distances between detection and ablation, often due to the time required between laser trigger and firing. ALABAMA exhibited a size-dependent HR of ~1% and ~75% for PSL of 200 and 400 nm, respectively (Brands et al., 2011), ATOFMS exhibited ~57% for 90 nm and ~ 93% for 290 nm PSL (Su et al., 2004), and the UoM LAAPTOF had maximum HR of 70%. Note that miniSPLAT has defined HR differently than the other SPMSs, as the ratio of the number of usable mass spectra to the number of laser triggers (Zelenyuk et al., 2015). This definition is specific to miniSPLAT, due to the aforementioned dual data acquisition mode. In this paper the former, more general, definition of HR is used.

4) Mass spectra quality related parameters, e.g., mass resolution, dynamic range of the ion signals, and signal to noise ratio (SNR). The aforementioned size detection ranges and DE, as well as mass spectra obtained in FIN-01 are examined and compared in Section 3.1.

In order to reduce data complexity, so-called "clustering algorithms" have been used to classify / categorize particle mass spectra, i.e., groups of mass spectra that share spectral similarities. Examples of such clustering algorithms include k-means, fuzzy c-means, ART-2a neural network, and hierarchical clustering (Gross et al., 2010; Murphy et al., 2003; Reitz et al., 2016; Zelenyuk et al., 2006, 2008b). The methods used to analyze data collected by the SPMSs deployed during FIN-01 are summarized in Table 1. Because the individual methods have been previously published, we refrain from a detailed description of the different analysis algorithms to instead focus on comparing the resulting grouped data from FIN-01.

2.2 Ancillary instruments

Additional instruments used during FIN-01 included multiple condensation particle counters with different size ranges (CPC, TSI, Model 3010, 3022, and 3025), a scanning mobility particle sizer (SMPS, TSI, Inc., Model 3081 differential mobility analyzer, DMA, and Model 3010 CPC) and an aerodynamic particle sizer (APS, TSI Inc., Model 3321) to measure the particle size distributions.

2.3 Experiments

Experiments were conducted using two chambers at KIT: the 84 m^3 AIDA chamber and the 3.7 m^3 stainless steel aerosol preparation and characterization (APC) chamber (Möhler et al., 2001, 2003; Saathoff et al., 2003). The aerosol particles and associated generation methods are summarized in Table 2. The placement of SPMSs during FIN-01 was used to minimize

200   distance to the AIDA and APC chambers and is shown in ~~Fig. 1~~Fig. S1. Specific details of the coating experiments can be found in Bertozzi (2022).

A subset of experiments was termed "blind experiments" with a goal of comparing results from the SPMSs where the aerosol composition was not known by the instrument teams a priori. The blind experiments were conducted under the direction of
205   three referees, not associated with specific instrument teams. The referees added different particle types to the APC chamber and then collected results before disclosure of the chamber contents. The objective of the referees was to provide a range of mass spectral signatures and particle sizes. After injection, the SPMSs sampled the (unknown) particle mixture directly from APC chamber. Groups then provided results to the referees without discussion with referees or other teams. As shown in ~~Fig. 2~~Fig. 1, there were two blind experiment periods (P1 and P2), each with a duration of 2 to 3 h. The particle samples added at
210   the start of P1 were: α-pinene SOA, Argentinian soil dust, and elemental carbon soot (GSG generator; hereafter graphite soot). Prior to P2, particle-free air was added to the chamber (i.e., dilution) and more graphite soot was added. The number percentage of α-pinene SOA, Argentinian soil dust, and graphite soot were approximately 24%, 41%, and 35%, respectively, in P1. After dilution and soot addition this mixture was (of α-pinene SOA, Argentinian soil dust, and graphite soot) 10%, 18%, and 72% in P2. The fractions were estimated based on (a) the total particle number concentration (C_n) measured by CPC, (b) an
215   assumption of equal wall loss rate for all the particles, and (c) an assumption of no formation of new particle types.

3 Results and discussions

3.1 SPMS performance

3.1.1 Particle size and detection efficiency

Polydisperse samples were used during FIN-01. The particle size measured by the SPMSs was d_{va} in the free molecular regime
220   (d_a measured by PALMS is assumed equivalent to d_{va}) while the ancillary instruments measured the electrical mobility diameter (d_m, SMPS) in the transition regime or aerodynamic diameter in continuum regime (d_{ca}, APS). The differences between d_{va}, d_{ca}, and d_m are due to non-unity density and non-spherical shape factors of the samples. A comprehensive discussion of the differences can be found e.g., in DeCarlo et al. (2004) and Slowik et al. (2004). To facilitate comparison, we converted d_m and d_{ca} to d_{va} using the following equations. It is assumed particles have no voids and slip correction is ignored:

$$d_{va} = d_m \times f_m = d_m \times \frac{\rho_p}{\rho_0 \chi_t \chi_v} \tag{1}$$

$$d_{va} = d_{ca} \times f_{ca} = d_{ca} \times \sqrt{\frac{\rho_p}{\rho_0}} \times \frac{\sqrt{\chi_c}}{\chi_v} \tag{2}$$

225   where ρ_0 is unit density (1 g cm⁻³), ρ_p is particle density and χ_c, χ_t, and χ_v are the dynamic shape factors (DSFs) in the continuum, transition, and free molecular regime, respectively. The values of the parameters used in this study are listed in

Table 2. f_m and f_{ca} are defined as the conversion factors for d_m and d_{ca}, respectively. Additional detail can be found in DeCarlo et al. (2004).

~~Figure 3~~Figure 2 shows the normalized particle size distributions measured by the SPMSs for the different particle types. The SPMSs all measured a similar size range, spanning parts of the accumulation (~0.1 to 1 µm) and coarse (> 1 µm) modes. The similar lower and upper cut-off sizes of ~100–200 nm and ~1–3 µm, respectively, were due to similar focusing inlets and similar wavelengths of detection lasers. The exception is LAAPTOF, which measured particles in a size range of ~450 nm to 2 µm d_{va} during FIN-01, most likely due to non-optimal detection laser alignment. Detection reduction at small and large particle sizes is due to light scattering and focusing of the particle beam, respectively (Bohren and Huffman, 1998; Schreiner et al., 1999).

Overall, the particle size distributions of the minerals (K-feldspar and illite NX) and dusts (desert and soil) measured by the SPMSs agreed reasonably well with those measured by the SMPS. The size measurements by the SPMSs and SMPS were not always as consistent as for the minerals and dusts. For Snomax this was most likely because of the broader size range, with half of the particles smaller than 100 nm d_{va} (i.e., beyond the typical lower size detection limit of SPMSs). Disagreement may also be attributed to the simplifications inherent in equations (1) and (2) or assumptions about the dynamic shape factors and/or particle density.

Another exception was the experiment with propane soot, for which most of the particles were smaller than the optical ~~below the~~ detection limit of most of the SPMSs. The conversion of SMPS data from d_m to d_{va} using equations (1) and (2) for propane soot was more uncertain than for the other particle types. Note that it is challenging to perform size conversions for aspherical particles; even for monodisperse (mass- or mobility-selected) particles, the d_{va} size distributions are broad and asymmetric due to the presence of particles with different shapes and/or orientation-dependent DSF in the free molecular regime (Beranek et al., 2012; Zelenyuk et al., 2008a). The propane soot particles in the experiments with high O:C ratio were compact and non-spherical, but not fractal, for which a conversion from d_m to d_{va} would be possible as discussed in previous studies (Naumann, 2003; Shapiro et al., 2012; Suski et al., 2021). Moreover, the size distribution of the soot particles evolved during the measurement due to aging/coagulation/compaction (Bhandari et al., 2019; Corbin et al., 2023). Size conversion of soot is beyond the focus of this study. A comprehensive discussion of physical and morphological parameters of soot particles can be found in the literature (Schneider et al., 2006; Shapiro et al., 2012; Sorensen, 2011; Suski et al., 2021).

~~Figure 4~~Figure 3 shows the DE, as a function of aerosol particle size and separated for each particle type, for the SPMSs. Given the different methodology applied for detection and mass spectral acquisition by miniSPLAT, we compare the results from the other SPMSs first. DE, a strong function of particle size, spans 2–3 orders of magnitude. PALMS exhibited the highest DE for all particle types, especially at the larger sizes (> 400 nm d_{va}). At sub-micrometer diameters, ALABAMA and ATOFMS exhibited comparable DE. This aligns with the respective size ranges corresponding to DE_{max} for PSL for each instrument (Table 1). As mentioned previously, LAAPTOF tended to measure relatively larger particles (> 500 nm) more effectively. Note that particle type also played a role in particle detection, most likely related to a composition dependent shape factor and/or light scattering efficiency. DE for propane soot particles is not shown in Fig. 4 due to the aforementioned low C_n within

the detectable size range of the SPMSs and the difficulty of size conversion. MiniSPLAT exhibited relatively higher DE than the other SPMSs. As previously mentioned, miniSPLAT has defined DE and HR differently in the literature than for the other SPMSs. Using the same definitions as the other SPMSs, for the corresponding measurements by miniSPLAT in Fig. 4, DE was ~38% of the whole size distribution while HR was ~11%. As an example in Fig 4a), both whole size distribution and mass spectra related DEs are shown to demonstrate the upper and lower limits of miniSPLAT DE.

3.1.2 Mass spectra

Examples of average mass spectra, normalized to maximum ion signal (peak area), for the polydisperse aerosol samples are shown in ~~Fig. 5~~Fig. 4 (Snomax) and ~~Fig. 6~~Fig. 5 (Moroccan desert dust). These two aerosol types were chosen to illustrate the performance of the different instruments. Snomax is a chemically homogeneous aerosol (Kanji et al., 2017; Möhler et al., 2007; Murray and Liu, 2022). Thus, potential differences between the individual SPMSs due to composition-dependent ionization efficiency should be minimal. Desert dust particles, such as the Moroccan sample, are chemically more complex and diverse (Hoose and Möhler, 2012; Kandler et al., 2007; Kanji et al., 2017; Marsden et al., 2019; Murray et al., 2012; Murray and Liu, 2022). Average mass spectra for the other aerosol types are shown in Figs. S1–5. In general, the SPMSs had common markers for specific particle types which are summarized in Table 3.

To better compare the mass spectra and quantify commonalities and differences, we conducted a statistical analysis using Pearson's correlation coefficient, denoted hereafter as 'r'. The coefficient measures the strength and direction of a linear relationship between two variables or data sets, e.g., two average mass spectra. A value of r=1 and -1 indicate a perfect positive and negative linear relationship, respectively, whereas r=0 indicates no linear correlation. The average r for the average positive and negative mass spectra of the different aerosol types between the different instruments can be found in Table S1. The five instruments exhibited comparable markers and good correlation, defined here as a r > 0.6 (greater than 60% linear correlation). On average and across all samples, the r value for positive spectra $r_{avg-pos} = 0.74 \pm 0.12$ and for negative spectra $r_{avg-neg} = 0.67 \pm 0.22$.

~~Figure 7~~Figure 6 shows a detailed analysis where we compare the linear correlation coefficient of each SPMS with each other, differentiated by aerosol type. Among the sampled particle types, the strongest correlation was for Snomax, $r_{avg-pos} = 0.92 \pm 0.04$ and $r_{avg-neg} = 0.90 \pm 0.05$. This was a consequence of the aforementioned factors: 1) Snomax was chemically homogeneous, 2) all instruments exhibited common spectral markers with a similar pattern (~~Fig. 5~~Fig. 4) and 3) Snomax produced multiple ion markers, many of which were of high signal/intensity.

The second strongest correlation, in negative spectra, was found for the Moroccan desert dust (~~Fig. 7~~Fig. 6 and Table S1). The strong correlation was due to a strong silicate pattern (m/z 60 SiO_2^-, 76 SiO_3^-, and 77 $HSiO_3^-$; ~~Fig. 6~~Fig. 5). This was generally true for the desert (~~Fig. 6~~Fig. 5) and soil dusts (~~Fig. S1~~Fig. S2) which had many common markers in their mass spectra. Despite similar cation markers, the correlations for the positive spectra of the dusts were not as good as negative spectra (~~Fig. 7~~Fig. 6 c and d). The major peaks, e.g., 27 Al^+, and/or 39 K^+, and/or 56 Fe^+ in soil dust had a higher average intensity than markers in desert dust. It is worth noting that soil dusts exhibited more diversity of signal, consistent with their being internal mixtures of

minerals and organics, hence a more complex composition (Kögel-Knabner et al., 2008; O'Sullivan et al., 2014; Tobo et al.,

295   2014). As an example, negative spectral organic acids makers, e.g., 45 COOH$^-$, were found in soil dust but not in desert dust.

For the pure mineral samples, e.g., K-feldspar (~~Fig. S2~~Fig. S3) and illite NX (~~Fig. S3~~Fig. S4), all instruments had common

markers at m/z 23 Na$^+$, 27 Al$^+$, 39/41 K$^+$, 56 Fe$^+$, 60 SiO$_2^-$, 76 SiO$_3^-$, and 77 HSiO$_3^-$. Illite NX spectra also contained m/z 24

Mg$^+$. Nitrate and sulfate markers were found in the negative spectra measured by ALABAMA, especially for K-feldspar. They

were identified as instrument-specific contamination, from an unknown source. This resulted in poor linear correlations with

300   the other instruments.

For α-pinene SOA, the instruments showed strong correlations in their positive and negative spectra (~~Fig. 7~~Fig. 6 and Table

S1). Common features included m/z 12 C$^+$, 24 C$_2^+$ and 36 C$_3^+$, 39 C$_3$H$_3^+$, 41 C$_3$H$_5^+$, and 43 C$_3$H$_7^+$/C$_2$H$_3$O$^+$ (~~Fig. S4~~Fig. S5).

For α-pinene SOA-coated K-feldspar, the spectra were similar to (uncoated) K-feldspar but with additional organics markers

(~~Fig. S5~~Fig. S6). It is worth noting that the correlations for SOA-coated K-feldspar were better than SOA, especially in negative

305   spectra ($r_{avg-neg}$ = 0.73 ± 0.03 and 0.30 ± 0.29 for SOA coated K-felspar and SOA, respectively). This was likely due to minerals

having relatively stronger spectral patterns than organics.

Relatively poor correlations were found for propane soot ($r_{avg-pos}$ = 0.51 ± 0.23 and $r_{avg-neg}$ = 0.35 ± 0.26, average spectra in ~~Fig.

S6~~Fig. S7). This can be attributed to the small particle size and resulting low data quantity, e.g., only 30 and 73 spectra were

collected by the ATOFMS and by the PALMS instrument, respectively. For the other particle types, thousands of spectra were

310   typically used for averaging. Given multiple common spectral markers, i.e., pure carbon ions, C$_m^+$ and C$_m^-$ (the number of

carbon atoms, m, can reach >7), better correlation would be expected for soot particles with d_{va} > 200 nm.

One conclusion of this intercomparison is that, in general, spectra were comparable across instrument types. Spectra of particle

types with compounds that created distinct marker peaks compared better than particles of higher compositional diversity

which created spectra with less distinct patterns. There were cases where spectral patterns were instrument-specific, which

315   resulted in lower correlations, but in at least one case this appeared related to an instrument-specific contamination issue.

Correlation was largely independent of ionization laser wavelength, but some differences were apparent; for example, mineral

and desert dust samples in miniSPLAT and dust samples in ATOFMS did not produce similar positive spectra for the same

particle types (Figs. 5, S2, and S3, and the correlation results for positive spectra in ~~Fig. 7~~Fig. 6 a, b, and c).

Particle type cross-correlations are shown in ~~Fig. 8~~Fig. 7 to demonstrate each SPMS's ability to distinguish particle types.

320   Good correlations (r > 0.8 for most cases) were observed between similar particle types, namely mineral samples (K-feldspar

and illite NX) and dust samples (Moroccan desert dust and Argentinian soil dust). SOA was clearly separated, as was propane

soot. Snomax was not clearly separated from minerals (such as K-feldspar and illite NX) and dusts in the positive spectra due

to common marker peaks (e.g., m/z 23 Na$^+$ and 39 K$^+$), whereas it was distinguishable in negative spectra due to silicate

signatures, which were present for minerals and dusts, but not for Snomax. This highlights the importance of simultaneous

325   acquisition of spectra of both polarities (a significant limitation of monopolar instruments such as PALMS).

Another important aspect of mass spectra is dynamic range of ion signals and signal-to-noise ratio (SNR). A wider dynamic

range allows detecting and distinguishing ion signals of varying intensities. This enables identification of trace species,

providing useful information in tracking the source of particles (Murphy, 2007). In general, the SPMSs exhibited wide dynamic ranges and high SNRs in their mass spectra, but variations existed among different instruments. Taking Snomax as an example

330 (~~Fig. 5~~Fig. 4), the dynamic ranges of the SPMSs were ~10^3 and ~10^2 in positive and negative spectra, respectively. SNR values were similar (~10^4) in both positive and negative spectra of PALMS, miniSPLAT and ATOFMS. Relatively lower SNRs (~10^3) were found for ALAB$\underline{A}$MA and LAA$\underline{P}$TOF, with their positive spectra exhibiting higher SNR than negative ones.

3.2 Blind experiment comparisons

3.2.1 Particle detection and sizing

335 The two distinct measurement periods, P1 and P2, for the blind experiments were described previously. Unlike the propane soot used in the other experiments, the particles used in blind experiments were pure EC graphitic soot (Crawford et al., 2011). The total C_n during P1 was ~2000 to 3000 cm^{-3} and decreased to ~600 to 900 cm^{-3} during P2, after the dilution and soot addition described previously (~~Fig. 2~~Fig. 1).

As shown in ~~Fig. 9~~Fig. 8 a1) and a2), the size distributions measured by the ALABAMA and the ATOFMS were most

340 comparable. The smaller (sub-200 nm) and larger (> 500 nm) particles were best resolved by miniSPLAT and PALMS. PALMS resolved d_{va} >1.2 µm (based on a comparison with APS data; not shown). LAAPTOF utilized a "first laser mode" (i.e., the ionization laser was triggered immediately after particle detection by the first detection laser) during the blind experiments to obtain more spectra, and, as a result, did not record size information. The other SPMS measurements all agreed in the d_{va} range of ~200 to 800 nm. (~~Fig. 9~~Fig. 8 a1 and a2) show an increase in DE for most measurements as particle sizes

345 increased (~~Fig. 9~~Fig. 8 b1 and b2). With the exception of miniSPLAT, the normalized size distributions measured by the SPMSs in P1 and P2 do not have significant differences (~~Fig. 9~~Fig. 8 a1 and a2). All the DEs were higher in P2 (~~Fig. 9~~Fig. 8 b2) than P1 (~~Fig. 9~~Fig. 8 b1). The d_{va} size distributions measured by miniSPLAT extended to smaller sizes than the other instruments and exhibited a mode at ~35 nm (see the insert in ~~Fig. 9~~Fig. 8 a1 and a2), which corresponded to fractal soot particles. As previously mentioned, the d_{va} of fractal soot particles is nearly independent of mass and d_m and is instead

350 determined by the size of primary spherules that comprise fractal agglomerates. The fractal graphitic soot particles used in the blind test were shown to be comprised of primary spherules with diameter of 6.6 ± 1.7 nm (Wenzel et al., 2003). The d_{va} of the graphitic soot particles (~35 nm) is smaller than the d_m of these particles, which varied between 150 nm and 400 nm.

3.2.2 Identification of different particle types

Based on independent measurements and data analysis, the participants of the blind experiments identified different particle

355 types in the unknown aerosol mixture. Participants were only told that particles in the blind experiments had been used in the prior FIN-01 experiments but not the number of types, size distributions, or number densities. The number fractions of the identified particle types reported are shown in ~~Fig. 10~~Fig. 9. Five particle types, including α-pinene SOA (C1), α-pinene SOA-coated minerals (C2), minerals (K-feldspar and/or illite NX) (C3), dust (soil or mineral) (C4), and soot (C5), were identified

by the participants. Across both periods, all distinct particle types of the blind experiment, five were reported by PALMS, four by ALABAMA (C1, 3, 4 soil and 5) and ATOFMS (C1, 2, 3, and 5), three by miniSPLAT (C1, 4 soil, and 5) and two by LAAPTOF (C1 and 4 mineral). SOA fractions measured by PALMS, ALABAMA, and LAAPTOF showed general good agreement.

3.2.3 Discussion of blind experiment results

Size distribution and the DE results in the blind experiments were consistent with the size and size-dependent DE discussion in Section 3.1.1. Some disagreement between SMPS and SPMSs could result from the simplifications inherent in equations (1) and (2), and/or inaccurate assumptions about the dynamic shape factors and/or bulk density. The main difference between P1 and P2 was the addition of fresh soot particles (~~Fig. 2~~Fig. 1).

Of the different particle types present in the APC chamber during the blind experiments, all instruments identified α-pinene SOA. All instruments, with the exception of LAAPTOF, also identified soot. This is most likely due to the aforementioned LAAPTOF low HR at small sizes. The case of soil dust was more complicated. PALMS, ALABAMA, and miniSPLAT all identified different types of soil dust. LAAPTOF identified mineral dust but did not specify the type. ATOFMS identified a mixture of minerals (illite NX and K-feldspar). ALABAMA and PALMS also identified illite NX and K-feldspar, respectively. This highlights the ability of the SPMSs to generally identify minerals and dusts but ~~the inability~~ difficulties to accurately distinguish specifically between dust and mineral types (see discussion in Section 3.1.2). PALMS and ATOFMS both identified SOA-coated minerals, although this type was not added to the chamber. Such internally mixed particles most likely resulted from coagulation of the external mixture of α-pinene SOA with soil dust in the chamber. The identification of such internally mixed particles is important because it demonstrates SPMSs' capability to investigate processes such as particle aging on a particle-by-particle level. Note that ~~Fig. 10~~Fig. 9 shows two miniSPLAT-derived pie charts. The left pie chart corresponds to the same data presented by the other SPMSs, the total mass spectra acquired and assigned to various particle classes. The right pie chart, provided to the referees, uses the DE calibrations, determined by miniSPLAT for many particle types, including SOA, soot, and dust (Vaden et al., 2011). Such calibrations take into account particle beam divergence, which depends on particle composition, shape, and morphology. The applied DE calibrations yield the 2nd pie chart (Fig. 9 e right) which can be compared to the original particle mix (Fig. 1 and Fig.9 f1). Note that the other instrument groups did not produce a similar calibrated pie chart in this study, however, this can be achieved if similar calibration for multiple particle types was done by using the other SPMSs. Such calibration can also be achieved in the field but with larger uncertainties due to the chemical and morphology complexity of the ambient particles.

It is noteworthy that caution should be utilized in the interpretations of the presented pie charts. For example, all the instruments classified the majority of particles as SOA and identified less than 10% soot particles. These results were in the context of certain size range, i.e., ~100–200 nm to ~2–3 μm d_{va}. To obtain more accurate number fractions, composition and size-dependent DE need to be considered.

4 Conclusions and outlook

We present here an intercomparison of five different SPMSs during the FIN-01workshop at the AIDA facility in November 2014. Due to the common fundamental components of the instruments, there was a general agreement in sizing of samples and the mass spectra they produced.

Similar size ranges, typically from ~100–200 nm to ~2–3 μm d_{va}, were measured. Overall, DE was found to be instrument-specific and more dependent on particle size than particle type. This highlights the importance of characterizing the size dependence of DE.

The SPMSs exhibited a wide dynamic range (up to ~10^3) and high SNR (up to ~10^4) in mass spectra. Good linear correlations of spectra measured by different instruments were found ($r_{avg-pos}$ = 0.74 ± 0.12 and $r_{avg-neg}$ = 0.67 ± 0.22), with the best correlations for Snomax ($r_{avg-pos}$ = 0.92 ± 0.04 and $r_{avg-neg}$ = 0.90 ± 0.05). The lowest correlation was found for propane soot ($r_{avg-pos}$ = 0.51 ± 0.23 and $r_{avg-neg}$ = 0.35 ± 0.26) due to the low data quantity resulting from the size below the typical SPMS detection limit. Particle identification favored the bipolar instruments.

Instrument-specific ability to differentiate particle type was evaluated using both cross-correlations and validation in blind experiments. It is shown that all SPMSs were able to differentiate between SOA, soot, and soil dust, but had difficulties distinguishing between specific dusts/minerals. The results of the blind experiments show that SPMSs can detect changes in particle mixing state, which in our experiments likely resulted from coagulation of externally mixed particles. The results should help our community advance our understanding of such instruments and their potential for investigating atmospheric particles and processing.

~~In recent years, SPMSs have been continuously upgraded in both hardware (particle sampling, optical design, and mass spectrometer) and software (data acquisition and data analysis methods).~~ Since the FIN-01 workshop, participants and other groups have been improving SPMS hardware as well as data analysis processes and particle type retrievals. For example, the ALABAMA has been implemented with a newly developed ADL system, a delayed ion extraction, and better electric shielding, resulting in higher DE for a wider size range and seven times higher intensities of the cation signals (Clemen et al., 2020). The next generation of the PALMS (PALMS-NG) has been updated with better particle sampling and optical design, which allow for the measurement of a wider size range (~100 nm to > 3 μm) and higher DE for the smaller particles (1 to 3 orders of magnitude improvement for the size < 200 nm), and a bipolar s-shaped mass spectrometer with higher mass resolution (can reach > 1000, formerly ~200) (Jacquot et al., 2024). ~~For example, a~~A method for distinguishing K-feldspar from illite has been developed by Marsden et al. (2018) and subsequently used in analyzing ambient data (Marsden et al., 2019). Since not all the minerals have the same properties, e.g. ice nucleating ability (Atkinson et al., 2013), the capability to distinguish minerals is critical for the research field. Future investigations could consider improving our ability to further distinguish particles, minerals, and dusts specifically.

Particle mass quantification, unaddressed in this paper, is another important contemporary topic. At the time of FIN01, SPMSs were qualitative. Since then, effort has been put into improving quantification. Froyd et al. (2019) is one example where particle

425 type fractions measured by PALMS were propagated onto a size distribution obtained by a collocated optical particle spectrometer, thereby enabling the quantitation of particle number, surface area, volume, and mass concentrations. Such quantification techniques have been and can be used as a framework for other SPMSs. Since FIN01, SPMS measurements are now generally considered quantitative with uncertainties. ~~to~~Some achievements have been made in the SPMS community, but further studies are still in high demand. Therefore, a~~A~~ ~~new~~ future workshop could focus on quantification.

430 As new SPMSs, new software and data analysis methods are developed, we propose that intercomparison workshops in laboratory should continue, and ideally, should also include field activities due to complexity of ambient particles.

435 *Data availability.* All data used for the figures in this paper can be accessed at https://radar.kit.edu/radar/en/dataset/ZGLkxMLhgxxEHhkk?token=rgHxTfHgvyPJeZZAdQQq. The DOI of the dataset is: https://doi.org/10.35097/ZGLkxMLhgxxEHhkk and will be available upon publication (Shen et al., 2024).

Author contributions. XS analyzed data, produced tables and figures, and was the lead manuscript writer. DJC participated in
440 FIN-01, provided suggestions for the data interpretation and discussion, reviewed, and edited the manuscript. DMB, FM, NAM, JS, JW, MAZ, and AZ operated the SPMSs and did basic analysis of the data. HS contributed to the generation and coating of reference particles, particle size data and discussion. NH helped to coordinate the campaign. CM, DMM, and OM contributed as the referees in the blind experiments and provided scientific support for evaluating, interpretation and discussion of the results. DJC, OM, and PJD organized the FIN-01 workshop. HC gave general comments on this paper. All authors
445 contributed to the final text.

Competing interests. The authors declare that at least one of the (co-)authors is a member of the editorial board of Atmospheric Chemistry and Physics. The authors also have no other competing interests to declare.

450 *Special issue statements.* This article is part of the special issue "Fifth International Workshop on Ice Nucleation (FIN)".

Acknowledgements. The FIN-01 workshop was supported by the U.S. National Science Foundation grant no. AGS-1339264, and by the U.S. Department of Energy's Atmospheric System Research, an Office of Science, Office of Biological and Environmental Research program, under grant no. DE-SC0014487, and by the German Science Foundation DFG (FOR 1525
455 "INUIT"). Special thanks to the AIDA staff at KIT for operating the chambers and associated instrumentation, and general technical. We thank Susan Schmidt's work on operating the ALABAMA instrument and analyzing the data, Andreas Hünig for support during the measurements. We thank Berko Sierau and Ulrike Lohmann for their support with ATOFMS data analysis and employment. We also thank participants from other SPMS teams that participated in FIN-01 but did not provide

data for this manuscript: the ATOFMS team at the University of California, San Diego (UCSD), LAAPTOF team at Vienna University, the LAAPTOF team at Carnegie Mellon University (CMU), and the SPLAT team at Max Planck Institute for Chemistry (MPIC).

References

Alexander, J. M., Bell, D. M., Imre, D., Kleiber, P. D., Grassian, V. H., and Zelenyuk, A.: Measurement of size-dependent dynamic shape factors of quartz particles in two flow regimes, Aerosol Sci. Technol., 50, 870–879, https://doi.org/10.1080/02786826.2016.1200006, 2016.

Allen, J. O., Fergenson, D. P., Gard, E. E., Hughes, L. S., Morrical, B. D., Kleeman, M. J., Gross, D. S., Galli, M. E., Prather, K. A., and Cass, G. R.: Particle detection efficiencies of aerosol time of flight mass spectrometers under ambient sampling conditions, Environ. Sci. Technol., 34, 211–217, https://doi.org/DOI 10.1021/es9904179, 2000.

Allen, J. O., Bhave, P. V., Whiteaker, J. R., and Prather, K. A.: Instrument busy time and mass measurement using aerosol time-of-flight mass spectrometry, Aerosol Sci. Technol., 40, 615–626, https://doi.org/10.1080/02786820600754623, 2006.

Atkinson, J. D., Murray, B. J., Woodhouse, M. T., Whale, T. F., Baustian, K. J., Carslaw, K. S., Dobbie, S., O'Sullivan, D., and Malkin, T. L.: The importance of feldspar for ice nucleation by mineral dust in mixed-phase clouds, Nature, 498, 355–358, https://doi.org/10.1038/nature12278, 2013.

Bein, K. J., Zhao, Y. J., Pekney, N. J., Davidson, C. I., Johnston, M. V., and Wexler, A. S.: Identification of sources of atmospheric PM at the Pittsburgh Supersite - Part II: Quantitative comparisons of single particle, particle number, and particle mass measurements, Atmos. Environ., 40, S424–S444, https://doi.org/10.1016/j.atmosenv.2006.01.064, 2006.

Beranek, J., Imre, D., and Zelenyuk, A.: Real-Time Shape-Based Particle Separation and Detailed in Situ Particle Shape Characterization, Anal. Chem., 84, 1459–1465, https://doi.org/10.1021/ac202235z, 2012.

Bertozzi, B.: Ice nucleation ability of secondary aerosol particles at cirrus cloud conditions, Doctoral dissertation, Karlsruhe Institute of Technology, https://doi.org/10.5445/IR/1000146739, 2022.

Bertozzi, B., Wagner, R., Leisner, T., and Möhler, O.: Suppression of the heterogeneous ice nucleation ability of feldspar particles at cirrus formation conditions by atmospherically relevant coatings, in preparation, 2024.

Bhandari, J., China, S., Chandrakar, K. K., Kinney, G., Cantrell, W., Shaw, R. A., Mazzoleni, L. R., Girotto, G., Sharma, N., Gorkowski, K., Gilardoni, S., Decesari, S., Facchini, M. C., Zanca, N., Pavese, G., Esposito, F., Dubey, M. K., Aiken, A. C., Chakrabarty, R. K., Moosmüller, H., Onasch, T. B., Zaveri, R. A., Scarnato, B. V., Fialho, P., and Mazzoleni, C.: Extensive Soot Compaction by Cloud Processing from Laboratory and Field Observations, Sci. Rep., 9, 11824, https://doi.org/10.1038/s41598-019-48143-y, 2019.

Bohren, C. F. and Huffman, D. R.: Absorption and Scattering of Light by Small Particles, 1st ed., Wiley, https://doi.org/10.1002/9783527618156, 1998.

Brands, M., Kamphus, M., Böttger, T., Schneider, J., Drewnick, F., Roth, A., Curtius, J., Voigt, C., Borbon, A., Beekmann, M., Bourdon, A., Perrin, T., and Borrmann, S.: Characterization of a newly developed aircraft-based laser ablation aerosol mass spectrometer (ALABAMA) and first field deployment in urban pollution plumes over Paris during MEGAPOLI 2009, Aerosol Sci. Technol., 45, 46–64, https://doi.org/10.1080/02786826.2010.517813, 2011.

Cabalo, J., Zelenyuk, A., Baer, T., and Miller, R. E.: Two-Color Laser Induced Evaporation Dynamics of Liquid Aerosols Probed by Time-of-Flight Mass Spectrometry, Aerosol Sci. Technol., 33, 3–19, https://doi.org/10.1080/027868200410813, 2000.

Clemen, H.-C., Schneider, J., Klimach, T., Helleis, F., Köllner, F., Hünig, A., Rubach, F., Mertes, S., Wex, H., Stratmann, F., Welti, A., Kohl, R., Frank, F., and Borrmann, S.: Optimizing the detection, ablation, and ion extraction efficiency of a single-particle laser ablation mass spectrometer for application in environments with low aerosol particle concentrations, Atmos. Meas. Tech., 13, 5923–5953, https://doi.org/10.5194/amt-13-5923-2020, 2020.

Corbin, J. C., Modini, R. L., and Gysel-Beer, M.: Mechanisms of soot-aggregate restructuring and compaction, Aerosol Sci. Technol., 57, 89–111, https://doi.org/10.1080/02786826.2022.2137385, 2023.

Cornwell, G. C., McCluskey, C. S., Levin, E. J. T., Suski, K. J., DeMott, P. J., Kreidenweis, S. M., and Prather, K. A.: Direct Online Mass Spectrometry Measurements of Ice Nucleating Particles at a California Coastal Site, J. Geophys. Res. Atmos., 124, 12157–12172, https://doi.org/10.1029/2019JD030466, 2019.

Crawford, I., Möhler, O., Schnaiter, M., Saathoff, H., Liu, D., McMeeking, G., Linke, C., Flynn, M., Bower, K. N., Connolly, P. J., Gallagher, M. W., and Coe, H.: Studies of propane flame soot acting as heterogeneous ice nuclei in conjunction with single particle soot photometer measurements, Atmos. Chem. Phys., 11, 9549–9561, https://doi.org/10.5194/acp-11-9549-2011, 2011.

Cziczo, D. J. and Froyd, K. D.: Sampling the composition of cirrus ice residuals, Atmospheric Research, 142, 15–31, https://doi.org/10.1016/j.atmosres.2013.06.012, 2014.

Cziczo, D. J., DeMott, P. J., Brock, C., Hudson, P. K., Jesse, B., Kreidenweis, S. M., Prenni, A. J., Schreiner, J., Thomson, D. S., Murphy, D. M., and Tobias, H. J.: A method for single particle mass spectrometry of ice nuclei, Aerosol Sci. Technol., 37, 460–470, https://doi.org/10.1080/02786820300976, 2003.

Cziczo, D. J., Murphy, D. M., Hudson, P. K., and Thomson, D. S.: Single particle measurements of the chemical composition of cirrus ice residue during CRYSTAL-FACE, J. Geophys. Res. Atmos., 109, 2003JD004032, https://doi.org/10.1029/2003JD004032, 2004.

Cziczo, D. J., Thomson, D. S., Thompson, T. L., DeMott, P. J., and Murphy, D. M.: Particle analysis by laser mass spectrometry (PALMS) studies of ice nuclei and other low number density particles, Int. J. Mass Spec., 258, 21–29, https://doi.org/10.1016/j.ijms.2006.05.013, 2006.

Cziczo, D. J., Froyd, K. D., Gallavardin, S. J., Moehler, O., Benz, S., Saathoff, H., and Murphy, D. M.: Deactivation of ice nuclei due to atmospherically relevant surface coatings, Environ. Res. Lett., 4, https://doi.org/Artn 044013 10.1088/1748-9326/4/4/044013, 2009.

Cziczo, D. J., Froyd, K. D., Hoose, C., Jensen, E. J., Diao, M., Zondlo, M. A., Jessica, B. S., Twohy, C. H., and Murphy, D. M.: Clarifying the dominant sources and mechanisms of cirrus cloud formation, Science, 340, 1320–1324, https://doi.org/10.1126/science.1234145, 2013.

Cziczo, D. J., Ladino, L. A., Boose, Y., Kanji, Z. A., Kupiszewski, P., Lance, S., Mertes, S., and Wex H: Measurements of ice nucleating particles and ice residuals, Met. Monogr., 58, 8.1-8.13, https://doi.org/10.1175/AMSMONOGRAPHS-D-16-0008.1, 2017.

Davis, W. D.: Continuous mass spectrometric analysis of particulates by use of surface ionization, Environ. Sci. Technol., 11, 587–592, https://doi.org/10.1021/es60129a004, 1977.

DeCarlo, P. F., Slowik, J. G., Worsnop, D. R., Davidovits, P., and Jimenez, J. L.: Particle morphology and density characterization by combined mobility and aerodynamic diameter measurements. Part 1: Theory, Aerosol Sci. Technol., 38, 1185–1205, https://doi.org/10.1080/027868290903907, 2004.

535 DeCarlo, P. F., Kimmel, J. R., Trimborn, A., Northway, M. J., Jayne, J. T., Aiken, A. C., Gonin, M., Fuhrer, K., Horvath, T., Docherty, K. S., Worsnop, D. R., and Jimenez, J. L.: Field-deployable, high-resolution, time-of-flight aerosol mass spectrometer, Anal. Chem., 78, 8281–8289, https://doi.org/10.1021/ac061249n, 2006.

DeMott, P. J., Cziczo, D. J., Prenni, A. J., Murphy, D. M., Kreidenweis, S. M., Thomson, D. S., Borys, R., and Rogers, D. C.: Measurements of the concentration and composition of nuclei for cirrus formation, Proc. Natl. Acad. Sci. U.S.A., 100, 14655– 540 14660, https://doi.org/10.1073/pnas.2532677100, 2003.

DeMott, P. J., Mohler, O., Stetzer, O., Vali, G., Levin, Z., Petters, M. D., Murakami, M., Leisner, T., Bundke, U., Klein, H., Kanji, Z. A., Cotton, R., Jones, H., Benz, S., Brinkmann, M., Rzesanke, D., Saathoff, H., Nicolet, M., Saito, A., Nillius, B., Bingemer, H., Abbatt, J., Ardon, K., Ganor, E., Georgakopoulos, D. G., and Saunders, C.: Resurgence in Ice Nuclei Measurement Research, B. Am. Meteorol. Soc., 92, 1623–1635, https://doi.org/10.1175/2011BAMS3119.1, 2011.

545 DeMott, P. J., Mohler, O., Cziczo, D. J., Hiranuma, N., Petters, M. D., Petters, S. S., Belosi, F., Bingemer, H. G., Brooks, S. D., Budke, C., Burkert-Kohn, M., Collier, K. N., Danielczok, A., Eppers, O., Felgitsch, L., Garimella, S., Grothe, H., Herenz, P., Hill, T. C. J., Hohler, K., Kanji, Z. A., Kiselev, A., Koop, T., Kristensen, T. B., Kruger, K., Kulkarni, G., Levin, E. J. T., Murray, B. J., Nicosia, A., O'Sullivan, D., Peckhaus, A., Polen, M. J., Price, H. C., Reicher, N., Rothenberg, D. A., Rudich, Y., Santachiara, G., Schiebel, T., Schrod, J., Seifried, T. M., Stratmann, F., Sullivan, R. C., Suski, K. J., Szakall, M., Taylor, 550 H. P., Ullrich, R., Vergara-Temprado, J., Wagner, R., Whale, T. F., Weber, D., Welti, A., Wilson, T. W., Wolf, M. J., and Zenker, J.: The Fifth International Workshop on Ice Nucleation phase 2 (FIN-02): laboratory intercomparison of ice nucleation measurements, Atmos. Meas. Tech., 11, 6231–6257, https://doi.org/10.5194/amt-11-6231-2018, 2018.

Dragoneas, A., Molleker, S., Appel, O., Hünig, A., Böttger, T., Hermann, M., Drewnick, F., Schneider, J., Weigel, R., and Borrmann, S.: The realization of autonomous, aircraft-based, real-time aerosol mass spectrometry in the upper troposphere 555 and lower stratosphere, Atmos. Meas. Tech., 15, 5719–5742, https://doi.org/10.5194/amt-15-5719-2022, 2022.

Du, X., Xie, Q., Huang, Q., Li, X., Yang, J., Hou, Z., Wang, J., Li, X., Zhou, Z., Huang, Z., Gao, W., and Li, L.: Development and characterization of a high-performance single-particle aerosol mass spectrometer (HP-SPAMS), Atmos. Meas. Tech., 17, 1037–1050, https://doi.org/10.5194/amt-17-1037-2024, 2024.

Erdmann, N., Dell'Acqua, A., Cavalli, P., Gruning, C., Omenetto, N., Putaud, J. P., Raes, F., and Van Dingenen, R.: Instrument 560 characterization and first application of the single particle analysis and sizing system (SPASS) for atmospheric aerosols, Aerosol Sci. Technol., 39, 377–393, https://doi.org/10.1080/027868290935696, 2005.

Fergenson, D. P., Song, X. H., Ramadan, Z., Allen, J. O., Hughes, L. S., Cass, G. R., Hopke, P. K., and Prather, K. A.: Quantification of ATOFMS data by multivariate methods, Anal. Chem., 73, 3535–3541, https://doi.org/DOI 10.1021/ac010022j, 2001.

565 Friedman, B., Kulkarni, G., Beránek, J., Zelenyuk, A., Thornton, J. A., and Cziczo, D. J.: Ice nucleation and droplet formation by bare and coated soot particles, J. Geophys. Res., 116, D17203, https://doi.org/10.1029/2011JD015999, 2011.

Froyd, K. D., Murphy, D. M., Brock, C. A., Campuzano-Jost, P., Dibb, J. E., Jimenez, J.-L., Kupc, A., Middlebrook, A. M., Schill, G. P., Thornhill, K. L., Williamson, C. J., Wilson, J. C., and Ziemba, L. D.: A new method to quantify mineral dust and other aerosol species from aircraft platforms using single-particle mass spectrometry, Atmos. Meas. Tech., 12, 6209–6239, 570 https://doi.org/10.5194/amt-12-6209-2019, 2019.

Fuzzi, S., Baltensperger, U., Carslaw, K., Decesari, S., van Der Gon, H. D., Facchini, M. C., Fowler, D., Koren, I., Langford, B., Lohmann, U., Nemitz, E., Pandis, S., Riipinen, I., Rudich, Y., Schaap, M., Slowik, J. G., Spracklen, D. V., Vignati, E., Wild, M., Williams, M., and Gilardoni, S.: Particulate matter, air quality and climate: lessons learned and future needs, Atmos. Chem. Phys., 15, 8217–8299, https://doi.org/10.5194/acp-15-8217-2015, 2015.

575   Gaie-Levrel, F., Perrier, S., Perraudin, E., Stoll, C., Grand, N., and Schwell, M.: Development and characterization of a single particle laser ablation mass spectrometer (SPLAM) for organic aerosol studies, Atmos. Meas. Tech., 5, 225–241, https://doi.org/10.5194/amt-5-225-2012, 2012.

Gallavardin, S., Lohmann, U., and Cziczo, D.: Analysis and differentiation of mineral dust by single particle laser mass spectrometry, Int. J. Mass Spectrom., 274, 56–63, https://doi.org/10.1016/j.ijms.2008.04.031, 2008.

580   Gard, E., Mayer, J. E., Morrical, B. D., Dienes, T., Fergenson, D. P., and Prather, K. A.: Real-time analysis of individual atmospheric aerosol particles: Design and performance of a portable ATOFMS, Anal. Chem., 69, 4083–4091, https://doi.org/DOI 10.1021/ac970540n, 1997.

Gemayel, R., Hellebust, S., Temime-Roussel, B., Hayeck, N., Van Elteren, J. T., Wortham, H., and Gligorovski, S.: The performance and the characterization of laser ablation aerosol particle time-of-flight mass spectrometry (LAAP-ToF-MS), 585   Atmos. Meas. Tech., 9, 1947–1959, https://doi.org/10.5194/amt-9-1947-2016, 2016.

Gemayel, R., Temime-Roussel, B., Hayeck, N., Gandolfo, A., Hellebust, S., Gligorovski, S., and Wortham, H.: Development of an analytical methodology for obtaining quantitative mass concentrations from LAAP-ToF-MS measurements, Talanta, 174, 715–724, https://doi.org/10.1016/j.talanta.2017.06.050, 2017.

Gross, D. S., Gälli, M. E., Silva, P. J., and Prather, K. A.: Relative sensitivity factors for alkali metal and ammonium cations 590   in single particle aerosol time-of-flight mass spectra, Anal. Chem., 72, 416–422, https://doi.org/DOI 10.1021/ac990434g, 2000.

Gross, D. S., Atlas, R., Rzeszotarski, J., Turetsky, E., Christensen, J., Benzaid, S., Olson, J., Smith, T., Steinberg, L., and Sulman, J.: Environmental chemistry through intelligent atmospheric data analysis, Environ. Model. Softw., 25, 760–769, https://doi.org/10.1016/j.envsoft.2009.12.001, 2010.

595   Gunsch, M. J., May, N. W., Wen, M., Bottenus, C. L. H., Gardner, D. J., VanReken, T. M., Bertman, S. B., Hopke, P. K., Ault, A. P., and Pratt, K. A.: Ubiquitous influence of wildfire emissions and secondary organic aerosol on summertime atmospheric aerosol in the forested Great Lakes region, Atmos. Chem. Phys., 18, 3701–3715, https://doi.org/10.5194/acp-18-3701-2018, 2018.

Hatch, L. E., Pratt, K. A., Huffman, J. A., Jimenez, J. L., and Prather, K. A.: Impacts of aerosol aging on laser 600   desorption/ionization in single-particle mass spectrometers, Aerosol Sci. Technol., 48, 1050–1058, https://doi.org/10.1080/02786826.2014.955907, 2014.

Healy, R. M., Sciare, J., Poulain, L., Crippa, M., Wiedensohler, A., Prevot, A. S. H., Baltensperger, U., Sarda-Esteve, R., McGuire, M. L., Jeong, C. H., McGillicuddy, E., O'Connor, I. P., Sodeau, J. R., Evans, G. J., and Wenger, J. C.: Quantitative determination of carbonaceous particle mixing state in Paris using single-particle mass spectrometer and aerosol mass 605   spectrometer measurements, Atmos. Chem. Phys., 13, 9479–9496, https://doi.org/10.5194/acp-13-9479-2013, 2013.

Hoose, C. and Möhler, O.: Heterogeneous ice nucleation on atmospheric aerosols: a review of results from laboratory experiments, Atmos. Chem. Phys., 12, 9817–9854, https://doi.org/10.5194/acp-12-9817-2012, 2012.

Hünig, A., Appel, O., Dragoneas, A., Molleker, S., Clemen, H.-C., Helleis, F., Klimach, T., Köllner, F., Böttger, T., Drewnick, F., Schneider, J., and Borrmann, S.: Design, characterization, and first field deployment of a novel aircraft-based aerosol mass spectrometer combining the laser ablation and flash vaporization techniques, Atmos. Meas. Tech., 15, 2889–2921, https://doi.org/10.5194/amt-15-2889-2022, 2022.

IPCC: Climate Change 2021 – The Physical Science Basis: Working Group I Contribution to the Sixth Assessment Report of the Intergovernmental Panel on Climate Change, edited by: Masson-Delmotte, V., Zhai, P., Pirani, A., Connors, S.L., Péan, C., Berger, S., Caud, N., Chen, Y., Goldfarb, L., Gomis, M.I., Huang, M., Leitzell, K., Lonnoy, E., Matthews, J.B.R., Maycock, T.K., Waterfield, T., Yelekçi, O., Yu, R., and Zhou B., Cambridge University Press, Cambridge, United Kingdom and New York, NY, USA, In press., 1st ed., Cambridge University Press, https://doi.org/10.1017/9781009157896, 2021.

Jacquot, J. L., Shen, X., Abou-Ghanem, M., Froyd, K. D., Lawler, M., Schill, G. P., Slovacek, K., Thomson, D. S., Cziczo, D. J., and Murphy, D. M.: A new airborne single particle mass spectrometer: PALMS-NG, Aerosol Science and Technology, 1–17, https://doi.org/10.1080/02786826.2024.2331549, 2024.

Jeong, C. H., McGuire, M. L., Godri, K. J., Slowik, J. G., Rehbein, P. J. G., and Evans, G. J.: Quantification of aerosol chemical composition using continuous single particle measurements, Atmos. Chem. Phys., 11, 7027–7044, https://doi.org/10.5194/acp-11-7027-2011, 2011.

Kamphus, M., Ettner-Mahl, M., Klimach, T., Drewnick, F., Keller, L., Cziczo, D. J., Mertes, S., Borrmann, S., and Curtius, J.: Chemical composition of ambient aerosol, ice residues and cloud droplet residues in mixed-phase clouds: single particle analysis during the Cloud and Aerosol Characterization Experiment (CLACE 6), Atmos. Chem. Phys., 10, 8077–8095, https://doi.org/10.5194/acp-10-8077-2010, 2010.

Kandler, K., Benker, N., Bundke, U., Cuevas, E., Ebert, M., Knippertz, P., Rodríguez, S., Schütz, L., and Weinbruch, S.: Chemical composition and complex refractive index of Saharan Mineral Dust at Izaña, Tenerife (Spain) derived by electron microscopy, Atmos. Environ., 41, 8058–8074, https://doi.org/10.1016/j.atmosenv.2007.06.047, 2007.

Kanji, Z. A., Ladino, L. A., Wex, H., Boose, Y., Burkert-Kohn, M., Cziczo, D. J., and Krämer, M.: Overview of ice nucleating particles, Met. Monogr., 58, 1.1-1.33, https://doi.org/10.1175/AMSMONOGRAPHS-D-16-0006.1, 2017.

Kögel-Knabner, I., Guggenberger, G., Kleber, M., Kandeler, E., Kalbitz, K., Scheu, S., Eusterhues, K., and Leinweber, P.: Organo-mineral associations in temperate soils: Integrating biology, mineralogy, and organic matter chemistry, Z. Pflanzenernähr. Bodenk., 171, 61–82, https://doi.org/10.1002/jpln.200700048, 2008.

Köllner, F., Schneider, J., Willis, M. D., Klimach, T., Helleis, F., Bozem, H., Kunkel, D., Hoor, P., Burkart, J., Leaitch, W. R., Aliabadi, A. A., Abbatt, J. P. D., Herber, A. B., and Borrmann, S.: Particulate trimethylamine in the summertime Canadian high Arctic lower troposphere, Atmos. Chem. Phys., 17, 13747–13766, https://doi.org/10.5194/acp-17-13747-2017, 2017.

Lacher, L., Clemen, H.-C., Shen, X., Mertes, S., Gysel-Beer, M., Moallemi, A., Steinbacher, M., Henne, S., Saathoff, H., Möhler, O., Höhler, K., Schiebel, T., Weber, D., Schrod, J., Schneider, J., and Kanji, Z. A.: Sources and nature of ice-nucleating particles in the free troposphere at Jungfraujoch in winter 2017, Atmos. Chem. Phys., 21, 16925–16953, https://doi.org/10.5194/acp-21-16925-2021, 2021.

Li, L., Huang, Z. X., Dong, J. G., Li, M., Gao, W., Nian, H. Q., Fu, Z., Zhang, G. H., Bi, X. H., Cheng, P., and Zhou, Z.: Real time bipolar time-of-flight mass spectrometer for analyzing single aerosol particles, Int. J. Mass. Spectrom., 303, 118–124, https://doi.org/10.1016/j.ijms.2011.01.017, 2011.

645 Lin, Q. H., Zhang, G. H., Peng, L., Bi, X. H., Wang, X. M., Brechtel, F. J., Li, M., Chen, D. H., Peng, P. A., Sheng, G. Y., and Zhou, Z.: In situ chemical composition measurement of individual cloud residue particles at a mountain site, southern China, Atmos. Chem. Phys., 17, 8473–8488, https://doi.org/10.5194/acp-17-8473-2017, 2017.

Liu, P., Ziemann, P. J., Kittelson, D. B., and McMurry, P. H.: Generating particle beams of controlled dimensions and divergence: II. Experimental evaluation of particle motion in aerodynamic lenses and nozzle expansions, Aerosol Sci.
650 Technol., 22, 314–324, https://doi.org/Doi 10.1080/02786829408959749, 1995.

Lohmann, U., Lüönd, F., and Mahrt, F.: An Introduction to Clouds: From the Microscale to Climate, 1st ed., Cambridge University Press, https://doi.org/10.1017/CBO9781139087513, 2016.

Lu, D. W., Liu, Q., Yu, M., Yang, X. Z., Fu, Q., Zhang, X. S., Mu, Y. J., and Jiang, G. B.: Natural silicon isotopic signatures reveal the sources of airborne fine particulate matter, Environ. Sci. Technol., 52, 1088–1095,
655 https://doi.org/10.1021/acs.est.7b06317, 2018.

Marsden, N. A., Flynn, M. J., Taylor, J. W., Allan, J. D., and Coe, H.: Evaluating the influence of laser wavelength and detection stage geometry on optical detection efficiency in a single-particle mass spectrometer, Atmos. Meas. Tech., 9, 6051–6068, https://doi.org/10.5194/amt-9-6051-2016, 2016.

Marsden, N. A., Flynn, M. J., Allan, J. D., and Coe, H.: Online differentiation of mineral phase in aerosol particles by ion
660 formation mechanism using a LAAP-TOF single-particle mass spectrometer, Atmos. Meas. Tech., 11, 195–213, https://doi.org/10.5194/amt-11-195-2018, 2018.

Marsden, N. A., Ullrich, R., Möhler, O., Hammer, S. E., Kandler, K., Cui, Z., Williams, P. I., Flynn, M. J., Liu, D., Allan, J. D., and Coe, H.: Mineralogy and mixing state of north African mineral dust by online single-particle mass spectrometry, Atmos Chem Phys, 19, 2259–2281, https://doi.org/10.5194/acp-19-2259-2019, 2019.

665 May, N. W., Gunsch, M. J., Olson, N. E., Bondy, A. L., Kirpes, R. M., Bertman, S. B., China, S., Laskin, A., Hopke, P. K., Ault, A. P., and Pratt, K. A.: Unexpected contributions of sea spray and lake spray aerosol to inland particulate matter, Environ. Sci. Tech. Lett., 5, 405–412, https://doi.org/10.1021/acs.estlett.8b00254, 2018.

McKeown, P. J., Johnston, M. V., and Murphy, D. M.: On-line single-particle analysis by laser desorption mass spectrometry, Anal. Chem., 63, 2069–2073, https://doi.org/10.1021/ac00018a033, 1991.

670 Middlebrook, A. M., Murphy, D. M., Lee, S. H., Thomson, D. S., Prather, K. A., Wenzel, R. J., Liu, D. Y., Phares, D. J., Rhoads, K. P., Wexler, A. S., Johnston, M. V., Jimenez, J. L., Jayne, J. T., Worsnop, D. R., Yourshaw, I., Seinfeld, J. H., and Flagan, R. C.: A comparison of particle mass spectrometers during the 1999 Atlanta Supersite Project, J. Geophys. Res. Atmos., 108, D7, https://doi.org/doi:10.1029/2001jd000660, 2003.

Möhler, O., Nink, A., Saathoff, H., Schaefers, S., Schnaiter, M., Schöck, W., and Schurath, U.: The Karlsruhe aerosol chamber
675 facility AIDA: technical description and first results of homogeneous and heterogeneous ice nucleation experiments, https://doi.org/10.5170/CERN-2001-007.163, 2001.

Möhler, O., Stetzer, O., Schaefers, S., Linke, C., Schnaiter, M., Tiede, R., Saathoff, H., Krämer, M., Mangold, A., Budz, P., Zink, P., Schreiner, J., Mauersberger, K., Haag, W., Kärcher, B., and Schurath, U.: Experimental investigation of homogeneous freezing of sulphuric acid particles in the aerosol chamber AIDA, Atmos. Chem. Phys., 3, 211–223,
680 https://doi.org/10.5194/acp-3-211-2003, 2003.

Möhler, O., DeMott, P. J., Vali, G., and Levin, Z.: Microbiology and atmospheric processes: the role of biological particles in cloud physics, Biogeosciences, 4, 1059–1071, https://doi.org/10.5194/bg-4-1059-2007, 2007.

Möhler, O., Benz, S., Saathoff, H., Schnaiter, M., Wagner, R., Schneider, J., Walter, S., Ebert, V., and Wagner, S.: The effect of organic coating on the heterogeneous ice nucleation efficiency of mineral dust aerosols, Environ. Res. Lett., 3, 025007, https://doi.org/10.1088/1748-9326/3/2/025007, 2008.

Morrical, B. D., Fergenson, D. P., and Prather, K. A.: Coupling two-step laser desorption/ionization with aerosol time-of-flight mass spectrometry for the analysis of individual organic particles, J. Am. Soc. Mass Spectrom., 9, 1068–1073, https://doi.org/10.1016/S1044-0305(98)00074-9, 1998.

Murphy, D. M.: The design of single particle laser mass spectrometers, Mass Spectrom. Rev., 26, 150–165, https://doi.org/10.1002/mas.20113, 2007.

Murphy, D. M. and Thomson, D. S.: Laser ionization mass-spectroscopy of single aerosol-particles, Aerosol Sci. Technol., 22, 237–249, https://doi.org/10.1080/02786829408959743, 1995.

Murphy, D. M., Middlebrook, A. M., and Warshawsky, M.: Cluster analysis of data from the Particle Analysis by Laser Mass Spectrometry (PALMS) instrument, Aerosol Sci. Technol., 37, 382–391, https://doi.org/10.1080/02786820300971, 2003.

Murphy, D. M., Hudson, P. K., Cziczo, D. J., Gallavardin, S., Froyd, K. D., Johnston, M. V., Middlebrook, A. M., Reinard, M. S., Thomson, D. S., Thornberry, T., and Wexler, A. S.: Distribution of lead in single atmospheric particles, Atmos. Chem. Phys., 7, 3195–3210, https://doi.org/10.5194/acp-7-3195-2007, 2007.

Murray, B. J. and Liu, X.: Ice-nucleating particles and their effects on clouds and radiation, in: Aerosols and Climate, Elsevier, 619–649, https://doi.org/10.1016/B978-0-12-819766-0.00014-6, 2022.

Murray, B. J., O'Sullivan, D., Atkinson, J. D., and Webb, M. E.: Ice nucleation by particles immersed in supercooled cloud droplets, Chem. Soc. Rev., 41, 6519, https://doi.org/10.1039/c2cs35200a, 2012.

Naumann, K.-H.: COSIMA—a computer program simulating the dynamics of fractal aerosols, J. Aerosol Sci., 34, 1371–1397, https://doi.org/10.1016/S0021-8502(03)00367-7, 2003.

Noble, C. A. and Prather, K. A.: Real-time single particle mass spectrometry: A historical review of a quarter century of the chemical analysis of aerosols, Mass Spectrom. Rev., 19, 248–274, https://doi.org/10.1002/1098-2787(200007)19:4<248::AID-MAS3>3.0.CO;2-I, 2000.

O'Sullivan, D., Murray, B. J., Malkin, T. L., Whale, T. F., Umo, N. S., Atkinson, J. D., Price, H. C., Baustian, K. J., Browse, J., and Webb, M. E.: Ice nucleation by fertile soil dusts: relative importance of mineral and biogenic components, Atmos. Chem. Phys., 14, 1853–1867, https://doi.org/10.5194/acp-14-1853-2014, 2014.

Passig, J., Schade, J., Rosewig, E. I., Irsig, R., Kröger-Badge, T., Czech, H., Sklorz, M., Streibel, T., Li, L., Li, X., Zhou, Z., Fallgren, H., Moldanova, J., and Zimmermann, R.: Resonance-enhanced detection of metals in aerosols using single-particle mass spectrometry, Atmos. Chem. Phys., 20, 7139–7152, https://doi.org/10.5194/acp-20-7139-2020, 2020.

Passig, J., Schade, J., Irsig, R., Kröger-Badge, T., Czech, H., Adam, T., Fallgren, H., Moldanova, J., Sklorz, M., Streibel, T., and Zimmermann, R.: Single-particle characterization of polycyclic aromatic hydrocarbons in background air in northern Europe, Atmos. Chem. Phys., 22, 1495–1514, https://doi.org/10.5194/acp-22-1495-2022, 2022.

Prather, K. A., Nordmeyer, Trent., and Salt, Kimberly.: Real-time characterization of individual aerosol particles using time-of-flight mass spectrometry, Anal. Chem., 66, 1403–1407, https://doi.org/10.1021/ac00081a007, 1994.

Pratt, K. A. and Prather, K. A.: Real-time, single-particle volatility, size, and chemical composition measurements of aged urban aerosols, Environ. Sci. Technol., 43, 8276–8282, https://doi.org/10.1021/es902002t, 2009.

720   Pratt, K. A. and Prather, K. A.: Mass spectrometry of atmospheric aerosols-Recent developments and applications. Part II: On-line mass spectrometry techniques, Mass Spectrom. Rev., 31, 17–48, https://doi.org/10.1002/mas.20330, 2012.

Qin, X. Y., Bhave, P. V., and Prather, K. A.: Comparison of two methods for obtaining quantitative mass concentrations from aerosol time-of-flight mass spectrometry measurements, Anal. Chem., 78, 6169–6178, https://doi.org/10.1021/ac060395q, 2006.

725   Ramisetty, R., Abdelmonem, A., Shen, X., Saathoff, H., Leisner, T., and Mohr, C.: Exploring femtosecond laser ablation in single-particle aerosol mass spectrometry, Atmos. Meas. Tech., 11, 4345–4360, https://doi.org/10.5194/amt-11-4345-2018, 2018.

Reilly, P. T. A., Lazar, A. C., Gieray, R. A., Whitten, W. B., and Ramsey, J. M.: The elucidation of charge-transfer-induced matrix effects in environmental aerosols via real-time aerosol mass spectral analysis of individual airborne particles, Aerosol 730   Sci. Technol., 33, 135–152, https://doi.org/10.1080/027868200410895, 2000.

Reinard, M. S. and Johnston, M. V.: Ion formation mechanism in laser desorption ionization of individual nanoparticles, J. Am. Soc. Mass Spectrom., 19, 389–399, https://doi.org/10.1016/j.jasms.2007.11.017, 2008.

Reitz, P., Zorn, S. R., Trimborn, S. H., and Trimborn, A. M.: A new, powerful technique to analyze single particle aerosol mass spectra using a combination of OPTICS and the fuzzy c-means algorithm, J. Aerosol Sci., 98, 1–14, 735   https://doi.org/10.1016/j.jaerosci.2016.04.003, 2016.

Riemer, N., Ault, A. P., West, M., Craig, R. L., and Curtis, J. H.: Aerosol Mixing State: Measurements, Modeling, and Impacts, Rev. Geophys., 57, 187–249, https://doi.org/10.1029/2018RG000615, 2019.

Rogers, D. C., DeMott, P. J., Kreidenweis, S. M., and Chen, Y.: Measurements of ice nucleating aerosols during SUCCESS, Geophys. Res. Lett., 25, 1383–1386, https://doi.org/10.1029/97GL03478, 1998.

740   Roth, A., Schneider, J., Klimach, T., Mertes, S., van Pinxteren, D., Herrmann, H., and Borrmann, S.: Aerosol properties, source identification, and cloud processing in orographic clouds measured by single particle mass spectrometry on a central European mountain site during HCCT-2010, Atmos. Chem. Phys., 16, 505–524, https://doi.org/10.5194/acp-16-505-2016, 2016.

Saathoff, H., Möhler, O., Schurath, U., Kamm, S., Dippel, B., and Mihelcic, D.: The AIDA soot aerosol characterisation campaign 1999, J. Aerosol Sci., 34, 1277–1296, https://doi.org/10.1016/S0021-8502(03)00363-X, 2003.

745   Saathoff, H., Naumann, K. H., Möhler, O., Jonsson, A. M., Hallquist, M., Kiendler-Scharr, A., Mentel, T. F., Tillmann, R., and Schurath, U.: Temperature dependence of yields of secondary organic aerosols from the ozonolysis of α-pinene and limonene, Atmos. Chem. Phys., 9, 1551–1577, https://doi.org/10.5194/acp-9-1551-2009, 2009.

Schade, J., Passig, J., Irsig, R., Ehlert, S., Sklorz, M., Adam, T., Li, C., Rudich, Y., and Zimmermann, R.: Spatially Shaped Laser Pulses for the Simultaneous Detection of Polycyclic Aromatic Hydrocarbons as well as Positive and Negative Inorganic 750   Ions in Single Particle Mass Spectrometry, Anal. Chem., 91, 10282–10288, https://doi.org/10.1021/acs.analchem.9b02477, 2019.

Schneider, J., Weimer, S., Drewnick, F., Borrmann, S., Helas, G., Gwaze, P., Schmid, O., Andreae, M. O., and Kirchner, U.: Mass spectrometric analysis and aerodynamic properties of various types of combustion-related aerosol particles, Int. J. Mass Spectrom., 258, 37–49, https://doi.org/10.1016/j.ijms.2006.07.008, 2006.

755 Schreiner, J., Schild, U., Voigt, C., and Mauersberger, K.: Focusing of aerosols into a particle beam at pressures from 10 to 150 Torr, Aerosol Sci. Technol., 31, 373–382, https://doi.org/Doi 10.1080/027868299304093, 1999.

Shapiro, M., Vainshtein, P., Dutcher, D., Emery, M., Stolzenburg, M., Kittelson, D. B., and McMurry, P. H.: Characterization of agglomerates by simultaneous measurement of mobility, vacuum aerodynamic diameter and mass, J. Aerosol Sci., 44, 24–45, https://doi.org/10.1016/j.jaerosci.2011.08.004, 2012.

760 Shen, X., Ramisetty, R., Mohr, C., Huang, W., Leisner, T., and Saathoff, H.: Laser ablation aerosol particle time-of-flight mass spectrometer (LAAPTOF): performance, reference spectra and classification of atmospheric samples, Atmos. Meas. Tech., 11, 2325–2343, https://doi.org/10.5194/amt-11-2325-2018, 2018.

Shen, X., Saathoff, H., Huang, W., Mohr, C., Ramisetty, R., and Leisner, T.: Understanding of atmospheric aerosol particles with improved particle identification and quantification by single particle mass spectrometry, Atmos. Meas. Tech., 12, 2219–
765 2240, https://doi.org/10.5194/amt-12-2219-2019, 2019.

Shen, X., Bell, D. M., Coe, H., Hiranuma, N., Mahrt, F., Marsden, N. A., Mohr, C., Murphy, D. M., Saathoff, H., Schneider, J., Wilson, J., Zawadowicz, M. A., Zelenyuk, A., DeMott, P. J., Möhler, O., and Cziczo, D. J.: Dataset for the paper entitled "The Fifth International Workshop on Ice Nucleation Phase 1 (FIN-01): Intercomparison of Single Particle Mass Spectrometers," https://doi.org/10.35097/ZGLkxMLhgxxEHhkk, 2024.

770 Sinha, M. P. and Friedlander, S. K.: Real-time measurement of sodium chloride in individual aerosol particles by mass spectrometry, Anal. Chem., 57, 1880–1883, https://doi.org/10.1021/ac00286a019, 1985.

Slowik, J. G., Stainken, K., Davidovits, P., Williams, L. R., Jayne, J. T., Kolb, C. E., Worsnop, D. R., Rudich, Y., DeCarlo, P. F., and Jimenez, J. L.: Particle Morphology and Density Characterization by Combined Mobility and Aerodynamic Diameter Measurements. Part 2: Application to Combustion-Generated Soot Aerosols as a Function of Fuel Equivalence Ratio, Aerosol
775 Sci. Technol., 38, 1206–1222, https://doi.org/10.1080/027868290903916, 2004.

Sorensen, C. M.: The Mobility of Fractal Aggregates: A Review, Aerosol Sci. Technol., 45, 765–779, https://doi.org/10.1080/02786826.2011.560909, 2011.

Su, Y. X., Sipin, M. F., Furutani, H., and Prather, K. A.: Development and characterization of an aerosol time-of-flight mass spectrometer with increased detection efficiency, Anal. Chem., 76, 712–719, https://doi.org/10.1021/ac034797z, 2004.

780 Sullivan, R. C., Petters, M. D., DeMott, P. J., Kreidenweis, S. M., Wex, H., Niedermeier, D., Hartmann, S., Clauss, T., Stratmann, Reitz, P., Schneider, J., and Sierau, B.: Irreversible loss of ice nucleation active sites in mineral dust particles caused by sulphuric acid condensation, Atmos. Chem. Phys., 10, 11471–11487, 2010.

Suski, K. J., Bell, D. M., Newburn, M. K., Alexander, M. L., Imre, D., Koppenaal, D. W., and Zelenyuk, A.: Real-time characterization of particles produced by laser ablation for analysis by inductively coupled plasma mass spectrometry,
785 Spectrochimica Acta Part B: Atomic Spectroscopy, 179, 106092, https://doi.org/10.1016/j.sab.2021.106092, 2021.

Thomson, D. S., Middlebrook, A. M., and Murphy, D. M.: Thresholds for laser-induced ion formation from aerosols in a vacuum using ultraviolet and vacuum-ultraviolet laser wavelengths, Aerosol Sci. Technol., 26, 544–559, https://doi.org/10.1080/02786829708965452, 1997.

Thomson, D. S., Schein, M. E., and Murphy, D. M.: Particle analysis by laser mass spectrometry WB-57F instrument overview,
790 Aerosol Sci. Technol., 33, 153–169, https://doi.org/10.1080/027868200410903, 2000.

Tobo, Y., DeMott, P. J., Hill, T. C. J., Prenni, A. J., Swoboda-Colberg, N. G., Franc, G. D., and Kreidenweis, S. M.: Organic matter matters for ice nuclei of agricultural soil origin, Atmos. Chem. Phys., 14, 8521–8531, https://doi.org/10.5194/acp-14-8521-2014, 2014.

Trimborn, A., Hinz, K.-P., and Spengler, B.: Online analysis of atmospheric particles with a transportable laser mass spectrometer, Aerosol Sci. Technol., 33, 191–201, https://doi.org/Doi 10.1080/027868200410921, 2000.

Vaden, T. D., Imre, D., Beranek, J., and Zelenyuk, A.: Extending the Capabilities of Single Particle Mass Spectrometry: II. Measurements of Aerosol Particle Density without DMA, Aerosol Sci Tech, 45, 125–135, https://doi.org/10.1080/02786826.2010.526156, 2011.

Wenzel, R. J., Liu, D. Y., Edgerton, E. S., and Prather, K. A.: Aerosol time-of-flight mass spectrometry during the Atlanta Supersite Experiment: 2. Scaling procedures, J. Geophys. Res. Atmos., 108, https://doi.org/Artn 8427 10.1029/2001jd001563, 2003.

Wex, H., Augustin-Bauditz, S., Boose, Y., Budke, C., Curtius, J., Diehl, K., Dreyer, A., Frank, F., Hartmann, S., Hiranuma, N., Jantsch, E., Kanji, Z. A., Kiselev, A., Koop, T., Möhler, O., Niedermeier, D., Nillius, B., Rösch, M., Rose, D., Schmidt, C., Steinke, I., and Stratmann, F.: Intercomparing different devices for the investigation of ice nucleating particles using Snomax® as test substance, Atmos. Chem. Phys., 15, 1463–1485, https://doi.org/10.5194/acp-15-1463-2015, 2015.

Woods, E., Smith, G. D., Dessiaterik, Y., Baer, T., and Miller, R. E.: Quantitative detection of aromatic compounds in single aerosol particle mass spectrometry, Anal. Chem., 73, 2317–2322, https://doi.org/10.1021/ac001166l, 2001.

Zawadowicz, M. A., Froyd, K. D., Murphy, D. M., and Cziczo, D. J.: Improved identification of primary biological aerosol particles using single-particle mass spectrometry, Atmos. Chem. Phys., 17, 7193–7212, https://doi.org/10.5194/acp-17-7193-2017, 2017.

Zawadowicz, M. A., Lance, S., Jayne, J. T., Croteau, P., Worsnop, D. R., Mahrt, F., Leisner, T., and Cziczo, D. J.: Quantifying and improving the optical performance of the Laser Ablation Aerosol Particle Time of Flight Mass Spectrometer (LAAPToF) instrument, Aerosol Sci Tech, https://doi.org/10.1080/02786826.2020.1724867, 2020.

Zelenyuk, A. and Imre, D.: Single particle laser ablation time-of-flight mass spectrometer: An introduction to SPLAT, Aerosol Sci. Technol., 39, 554–568, https://doi.org/10.1080/027868291009242, 2005.

Zelenyuk, A., Cabalo, J., Baer, T., and Miller, R. E.: Mass Spectrometry of Liquid Aniline Aerosol Particles by IR/UV Laser Irradiation, Anal. Chem., 71, 1802–1808, https://doi.org/10.1021/ac9809711, 1999.

Zelenyuk, A., Imre, D., Cai, Y., Mueller, K., Han, Y. P., and Imrich, P.: SpectraMiner, an interactive data mining and visualization software for single particle mass spectroscopy: A laboratory test case, Int. J. Mass Spectrom., 258, 58–73, https://doi.org/10.1016/j.ijms.2006.06.015, 2006.

Zelenyuk, A., Yang, J., Song, C., Zaveri, R. A., and Imre, D.: A New Real-Time Method for Determining Particles' Sphericity and Density: Application to Secondary Organic Aerosol Formed by Ozonolysis of α-Pinene, Environ. Sci. Technol., 42, 8033–8038, https://doi.org/10.1021/es8013562, 2008a.

Zelenyuk, A., Imre, D., Nam, E. J., Han, Y., and Mueller, K.: ClusterSculptor: Software for expert-steered classification of single particle mass spectra, Int. J. Mass Spectrom., 275, 1–10, https://doi.org/10.1016/j.ijms.2008.04.033, 2008b.

Zelenyuk, A., Yang, J., and Imre, D.: Comparison between mass spectra of individual organic particles generated by UV laser ablation and in the IR/UV two-step mode, Int. J. Mass Spectrom., 282, 6–12, https://doi.org/10.1016/j.ijms.2009.01.015, 2009a.

830   Zelenyuk, A., Yang, J., Choi, E., and Imre, D.: SPLAT II: An aircraft compatible, ultra-sensitive, high precision instrument for in-situ characterization of the size and composition of fine and ultrafine particles, Aerosol. Sci. Technol., 43, 411–424, https://doi.org/10.1080/02786820802709243, 2009b.

Zelenyuk, A., Imre, D., Wilson, J., Zhang, Z., Wang, J., and Mueller, K.: Airborne Single Particle Mass Spectrometers (SPLAT II & miniSPLAT) and New Software for Data Visualization and Analysis in a Geo-Spatial Context, J. Am. Soc. Mass Spectrom., 26, 257–270, https://doi.org/10.1007/s13361-014-1043-4, 2015.

835   Zenobi, R. and Knochenmuss, R.: Ion formation in MALDI mass spectrometry, Mass Spectrom. Rev., 17, 337–366, https://doi.org/Doi 10.1002/(Sici)1098-2787(1998)17:5<337::Aid-Mas2>3.0.Co;2-S, 1998.

Zhou, Y., Huang, X. H. H., Griffith, S. M., Li, M., Li, L., Zhou, Z., Wu, C., Meng, J. W., Chan, C. K., Louie, P. K. K., and Yu, J. Z.: A field measurement based scaling approach for quantification of major ions, organic carbon, and elemental carbon using a single particle aerosol mass spectrometer, Atmos. Environ., 143, 300–312,
840   https://doi.org/10.1016/j.atmosenv.2016.08.054, 2016.

Table 1: SPMSs, performance parameters, and data analysis methods

	PALMS	ALABAMA	miniSPLAT	LAAPTOF (AeroMegt, Germany)	ATOFMS (TSI 3800-100, USA)
Affiliation	MIT	MPIC	PNNL	UoM	ETH
Inlet Flowrate (cm^3 min^{-1})	ADL 400	ADL 80	ADL 100	ADL 100	ADL 100
Detection and sizing	One Nd:YAG laser Two beams (532 nm, 50 mW, beam width: 1st 200 μm, 2nd 100 μm)	One laser diode Two beams (405 nm, 50 mW, beam width: 190 μm)	Two Nd:YAG lasers (532 nm, 300 mW, beam width: 330 μm)	Two laser diodes (405 nm, 40 mW, beam width:> 50 μm)	Two ~~laser diodes~~Nd:YAG laser (405 nm, 95 mW, beam width: ~ 0.5 mm)
LDI	One step ArF Excimer laser (193 nm, 3–5 mJ/pulse, pulse duration: 4 ns, beam width: 150 μm at focal spot; beam direction: perpendicular to particle beam)	One step Nd:YAG laser (266 nm, 3-4 mJ/pulse, pulse duration: 5.2 ns, beam width: 250 μm, beam direction: facing particle beam)	One step ArF Excimer laser (193 nm, 0.5–2 mJ/pulse, pulse duration: 8 ns, beam focal spot: 550 × 750 μm, laser beam direction: sideways to the particle beam)	One step ArF Excimer laser (193 nm, 4 mJ/pulse, pulse duration: 6–8 ns, beam width: 300 μm, beam direction: facing particle beam)	One step Nd:YAG laser (266 nm, max 5 mJ/pulse, but 1.1–1.2 mJ/pulse in FIN-01, pulse duration: 5 ns, beam width: 2.4 mm; beam direction: perpendicular to particle beam)
Distances	Inlet exit – 1st laser's focal point: 55 mm 1st – 2nd lasers: 34 mm 2nd – 3rd lasers: 100 μm	90.5 mm 70 mm N/A	N/A 109 mm N/A	N/A 113 mm N/A	N/A 6~~0 cmmm~~ 12~~0 cmmm~~
MS	Unipolar TOF (Switchable polarity)	Bipolar TOF	Bipolar TOF	Bipolar TOF	Bipolar TOF
Size range	200 nm – 3 μm d_{va}	200 nm – 1 μm d_{va}	50 nm – 1.4 μm d_m	200 nm – 3 μm d_{va}	100 nm – 3 μm d_{va}
DE for PSL	min: 0.1 % (150 nm) max: 10% (300 nm – 1 μm d_{va})	0.3% (200 nm) 86% (400 nm)	~0.02% (50 nm d_m)[b] ~100% (125 – 600 nm d_m)	max=1% at 600 nm (UoM LAAPTOF)	0.5% (90 nm) 47.4 % (290 nm)
HR for PSL	~95% (no obvious size dependent and not limited to spherical particles, e.g., PSL)	min: ~1% (200 nm) max: ~75% (400 nm)	~100%[b] (125 – 600 nm)	max: ~70% (UoM LAAPTOF)	~57% (90 nm) ~93% (290 nm)
Mass resolution	~200 (max)	Between 100 and 600, ~400 for m/z 200	N/A	>600 at m/z 184	~500 for m/z 1 to 800
Classification method	Hierarchical cluster algorithm & Target-oriented particle typing	Fuzzy c means clustering	K-means clustering	Fuzzy c-means clustering	ART-2a algorithm Other classification methods available as part of e.g., FATES
References[a]	Cziczo et al., 2006	Brands et al., 2011 Schmidt et al., 2017	[b]Zelenyuk et al., 2015	Gemayel et al., 2016 Marsden et al., 2016 Shen et al., 2018	Prather et al., 1994 Gard et al., 1997 Su et al., 2004

[a]Note that the references for the commercial instruments are not limited to the specific ones used in this study. [b]Note that the terminology in DE and HR in the miniSPLAT reference is different from the other SPMSs (see text for details).

845

Table 2: Aerosol types, properties, composition, and generation techniques

Aerosol type	Density[a] (g cm^{-3})	DSF[a] (χ_c; χ_t; χ_v)	Composition	Generation method	AIDA Exp #	ACP Exp #
K-feldspar (FS01)	2.56	1.2; 1.2; 1.5	FS01: microcline 76%, albite 24%	Rotating brush (PALAS, RGB1000)		6
Illite NX	2.65	1.4; 1.4; 1.9	illite 69%, kaolinite 10%, calcite 3%, quartz 3%, feldspar (orthoclase/sanidine) 14%	Rotating brush (PALAS, RGB1000)		13, 21
Desert dust[b] (Moroccan)	2.50	1.5; 1.5; 1.8	Quartz 50-60%, illite (<10% total feldspar), iron oxide, calcite, and doromite	Rotating brush (PALAS, RGB1000)	20	26
Soil dust (Argentinian)	2.60	1.4; 1.4; 2.0	Mixture of minerals and organics	Rotating brush (PALAS, RGB1000)	48	25, 29
Propane soot	1.40	1.8; 1.8; 2.8	Elemental carbon (EC) and Organic carbon (OC)	Propane burner (RSG miniCAST; Jing Ltd) Incomplete combustion of propane, C/O=0.54		14
Graphite soot	2.26	2.8; 2.8; 5.0	Pure EC	Graphite spark generator from Palas (GSG 1000)		29
α-pinene SOA[c]	1.25	1.0; 1.0; 1.0	Complex mixture of mainly organic acids and aldehydes	In situ formation from ozonolysis of a-pinene (nucleation and condensation growth)		27, 29
SOA-coated K-feldspar (FS04)	N/A	N/A	α-pinene SOA and FS04 FS04: microcline 80%, albite 18%, quartz 2%	In situ formation from ozonolysis of α-pinene and condensation to dust particles	46	
Snomax[c]	1.35	1.0; 1.0; 1.0	protein complexes from nonviable *Pseudomonas syringae* bacteria	Atomizer (TSI, 3076)		16, 17, 22

[a]For most of the particle samples, the particle density and DSF in transitional and free molecular flow regimes, χ_t and χ_v, were obtained from the measurements by miniSPLAT during FIN-01 as described in Alexander et al. (2016). χ_t is near the continuum flow limit, for simplicity we assume χ_c (not measured) is equal to χ_t. [b]For desert dust, particle density and DSF is described in Froyd et al. (2019). [c]For α-pinene SOA and Snomax sphericity is assumed ($\chi_c = \chi_t = \chi_v = 1$), therefore the densities shown here are the effective density. Additional detail can be found in Zelenyuk (2008a), Saathoff et al. (2009) and Wex et al. (2015), respectively.

850

 Table 3: Particle types and the corresponding mass spectral markers

Particle type	Markers_cations	Markers_anions	Specific patterns	Other potential ions
K-feldspar	23 Na, 27 Al, 39&41 K (28 Si, 44 SiO)*	60 SiO_2, 76 SiO_3, 77 $HSiO_3$ (43 AlO, 88 Si_2O_2, 103 (AlO)SiO2, 119 AlSiO4, 136 $(SiO_2)_2O$, 148$(SiO_2)_2$Si, 179 $AlSiO_4.SiO_2$)		7 Li, 56 Fe, 63 & 65 Cu, 64 & 66 Zn, 85 & 87 Rb, 133 Cs (PALMS), 137 & 138 Ba, 153 &154 BaO
Illite NX	23 Na, 24 Mg, 27 Al, 56 Fe, 39&41 K (28 Si, 44 SiO)	43 AlO, 60 SiO_2, 76 SiO_3, 77 $HSiO_3$, 88 Si_2O_2, 103 (AlO)SiO2, 119 AlSiO4, 136 $(SiO_2)_2O$, 148$(SiO_2)_2$Si, 179 $AlSiO_4.SiO_2$ 63 PO_2, 79 PO_3		7 Li, 63 & 65 Cu, 64 & 66 Zn, 85 & 87 Rb, 133 Cs (PALMS), 137 & 138 Ba, 153 &154 BaO,
Desert dust (Moroccan)	7 Li, 23 Na, 24 Mg, 27 Al, 39&41 K, 56 Fe (28 Si, 44 SiO); (40 Ca, 56 CaO, 72 CaO_2, 96 Ca_2O, 112 $(CaO)_2$); (63 & 65 Cu, 64 & 66 Zn, 85 & 87 Rb, 137 & 138 Ba, 153 &154 BaO)	26 CN or C_2H_2, 42 CNO or C_2H_2O, 43 AlO, 60 SiO_2, 76 SiO_3, 77 $HSiO_3$, 88 Si_2O_2, 97 HSO_4, 103 (AlO)SiO2, 119 AlSiO4, 136 $(SiO_2)_2O$ (148$(SiO_2)_2$Si, 179 $AlSiO_4.SiO_2$)		133 Cs (PALMS) 45 COOH, 71 CCH_2COOH 63 PO_2, 79 PO_3
Soil dust (Argentinian)	similar as desert dust	In addition to the markers of MD, there are organic acids related ones 45 COOH, 71 CCH_2COOH (89 (CO)OCOOH)	Distinguish desert and soil dusts: soil dust has organic acids, less intensive silicate pattern, and more intensive anion pairs of m/z 26⁻ & 42⁻ and 63⁻ & 79⁻	
Soot with org (Propane soot)	EC fragments: C_m OC fragments: 39 C_3H_3, 56 C_4H_8 (27 C_2H_3, 28 CO, 40 C_2O, 41 C_3H_5, 44 COO, 50 C_4H_2, 69 C_5H_9)	EC fragments: C_m OC fragments: 26 C_2H_2, 42 C_2H_2O	"One fork shape" at m/z 12⁺, 24⁺, 36⁺ EC pattern is more intensive than OC fragments	
α-pinene SOA	mainly C_xH_y and $C_xH_yO_z$ fragments: e.g., 12 C, 13 CH, 15 CH_3, 19 H_3O, 24 C_2, 27 C_2H_3, 28 CO, 36 C_3, 39 C_3H_3, 41 C_3H_5, 43 C_3H_7 or C_2H_3O, 55 C_4H_7/C_3H_3O, 59 C_2H_2OOH, 69 C_5H_9, 77 C_6H_5, 83 $C_6H_{10}/C_5H_7O/C_4H_2OOH$, 85 C_7H_5, 91 C_7H_7, 95 C_7H_{11}	mainly organic acids fragments: e.g., $(CH_2)_{n=0-11}$ COOH: 45 to 199 $(CH_2)_{n=0-10}$ CCOOH: 57 to 197 $(CH_2)_{n=0-4}$ (CO)OCOOH: 89 to 145 (Only for PALMS and LAAPTOF)	"Two fork shapes" m/z 12⁺, 24⁺, 36⁺ & 39⁺, 41⁺, 43⁺	
Snomax	23 Na, 30 NO, 39 K or C_3H_3, 41 K or C_3H_5, 47 PO, 56 Fe or C_4H_8, 62 Na_2O, 70 C_5H_{10}, 72 FeO, 78 Na_2O_2 165 Na_3SO_4, 181 Na_2SO_4NaO or $C_4H_7O_4NO_3$, 197 NaK_2SO_4 (18 NH_4, 28 CO, 44 CO_2, 86 $(C_2H_5)_2NCH_2$,213 K_3SO_4)	26 CN or C_2H_2, 42 CNO or C_2H_2O 45 COOH, 59 CH_3COOH, 71 CCH_2COOH 63 PO_2, 79 PO_3, 96 SO_4, 97 HSO_4, 119 $NaSO_4$ (135 KSO_4, 153 Na_2Cl_3)	Phosphate fragments at both pos and neg Important pairs m/z 23⁺&39⁺; 18⁺&30⁺ 26⁻&42⁻; 63⁻&79⁻	

Note: ions in parenthesis are not observed in all SPMS mass spectra.
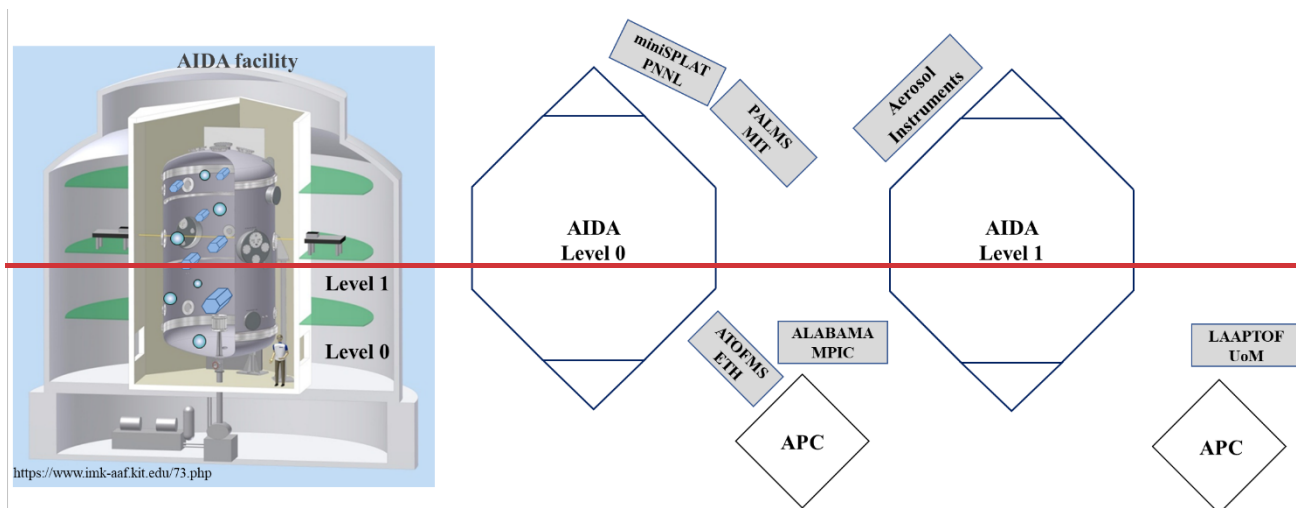
Figure 1: Experimental setup. During the campaign the instruments were positioned to minimize the length of the sampling lines to 860 **the AIDA and APC chambers. The sampling lines were 6 × 4 mm (OD × ID) stainless steel tubing.**
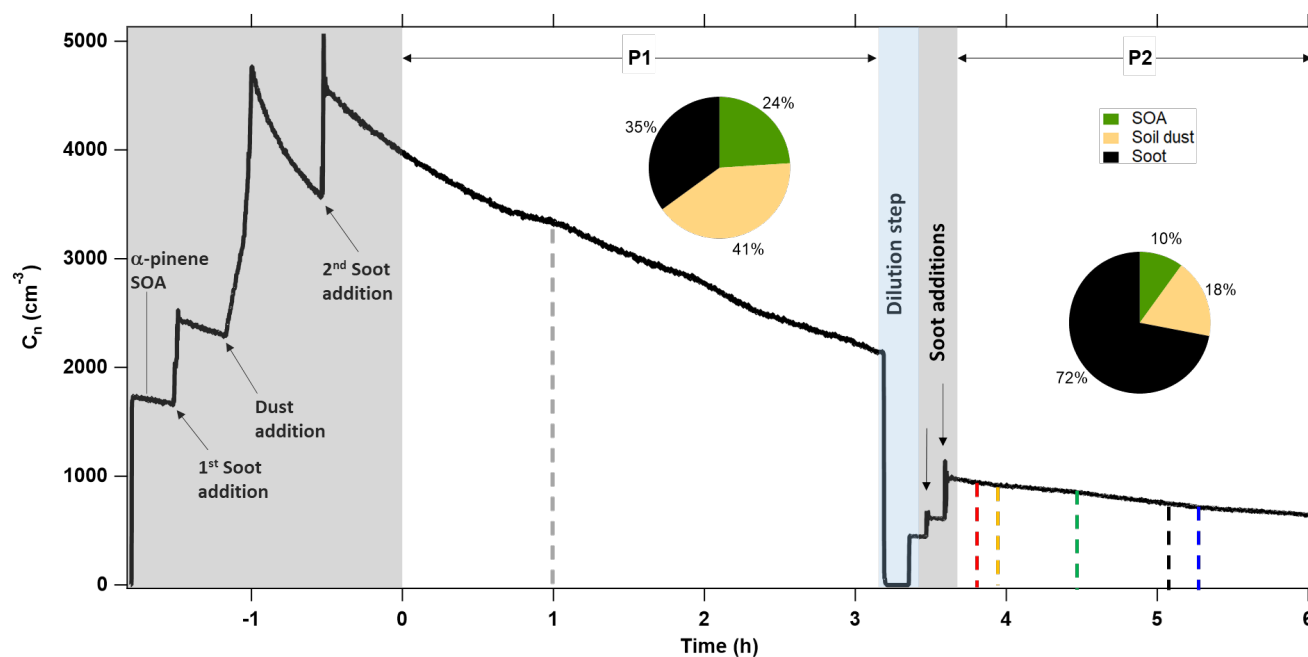
Figure 21: Time series of total particle C_n measured by a CPC in the APC chamber during the blind experiments. SPMS 865 **measurements were conducted during two periods, P1 and P2. In P1, the SPMSs started sampling at the same time (grey dashed line), except miniSPLAT which started 15 min later. In P2, sampling started at different times (red, orange, green, black and blue dashed lines are for PALMS, ATOFMS, LAAPTOF, miniSPLAT and ALABAMA, respectively). The pie charts denote particle types and their number fractions in P1 and P2, respectively. Note that the grey and blue shaded areas denote the aerosol mixture preparation periods, and a dilution step when the chamber was partly pumped out and refilled with clean air.**
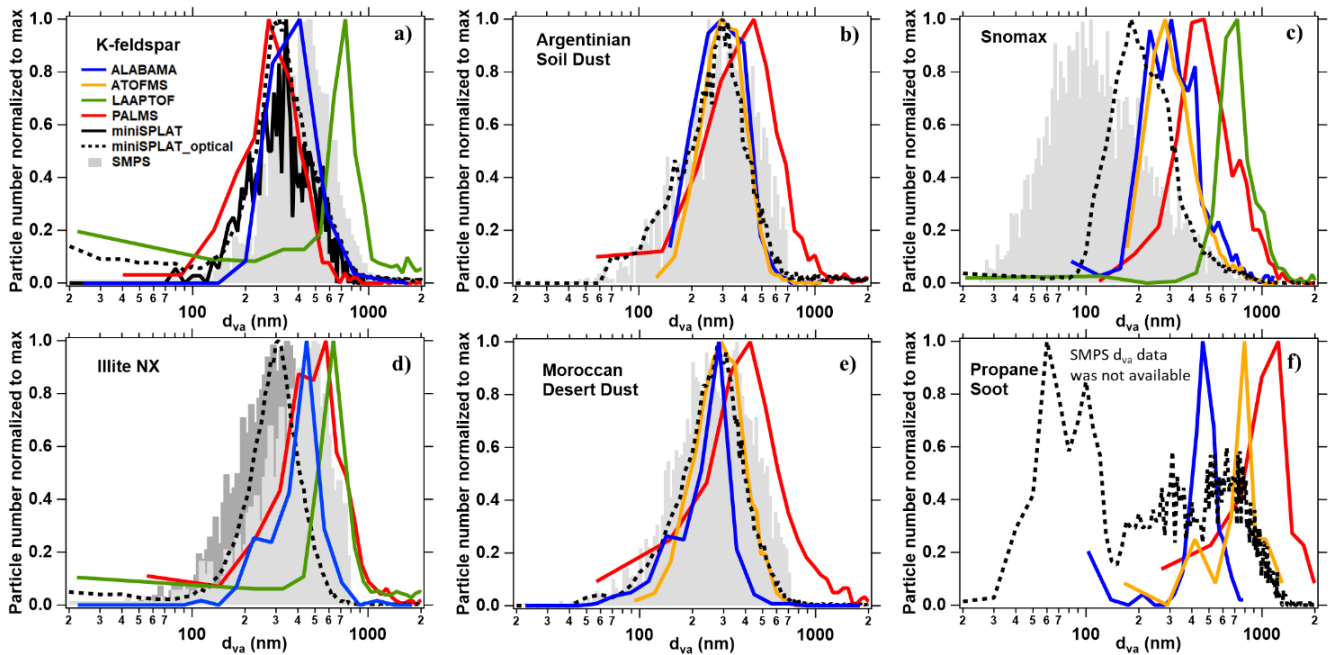
870

Figure ~~3~~2: SPMS size distributions (normalized to maximum particle number) for selected particle types, i.e., a) K-feldspar, b) Argentinian soil dust, c) Snomax, d) Illite NX, e) Moroccan desert dust, and f) Propane soot. Color codes correspond to d_{va} measured by ALABAMA (blue), ATOFMS (orange), LAAPTOF (green), PALMS (red), and miniSPLAT (black). Note that the dashed black curves represent the DE of the size distribution measured by miniSPLAT, while in a) the solid black curve represents DE consistent

875   with the other SPMSs (see text for details). Particle sizes measured by the SMPS over a scan range of 14–820 nm d_m was converted to d_{va} (grey) for comparison. For illite NX particles, two different SMPS size distributions from the APC13 and APC21 experiments are shown in light and dark, respectively (miniSPLAT result was from only APC21, while the others were from APC13). For soot particles, the SMPS d_{va} data was not available for these experiments (see text for details). Dashed lines in d) are used to emphasize the extent of the distributions. In most cases the particle numbers by each SPMS (used to derive the distribution curves) were

880   hundreds to thousands. The exception is propane soot, for which most of SPMSs detected < 100 particles due to the detection limit.
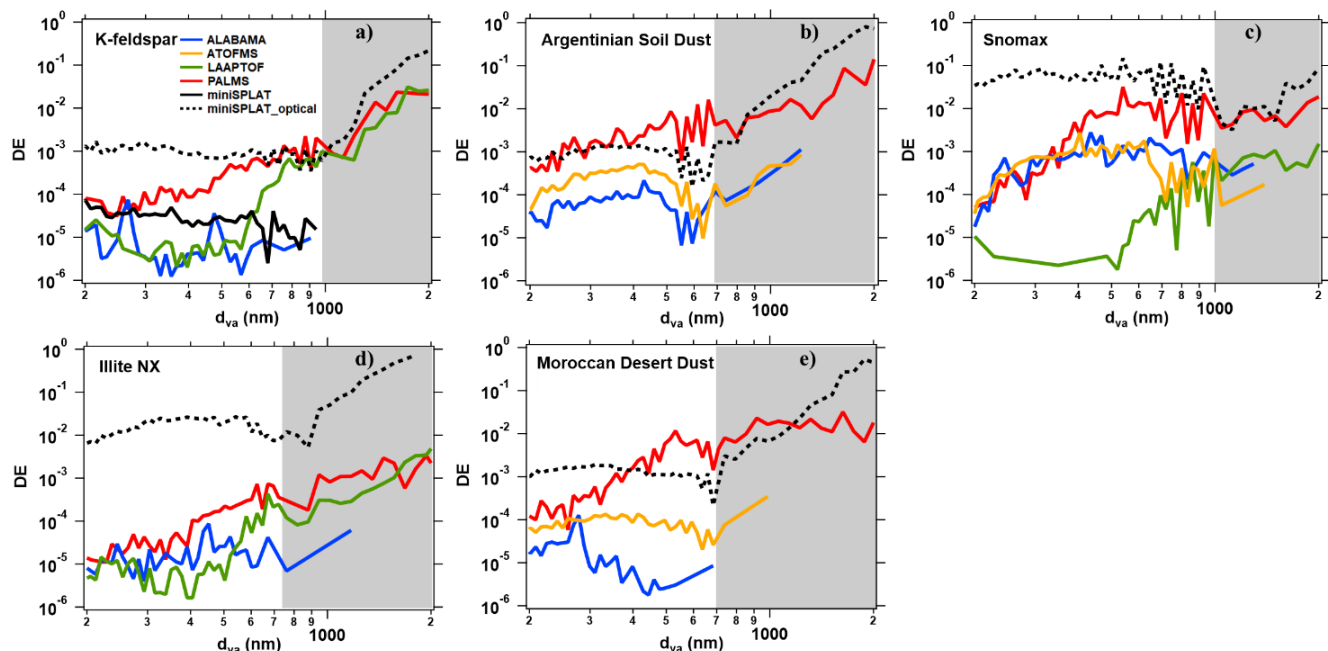
Figure 43: Detection efficiencies of SPMSs for selected particle types, i.e., a) K-feldspar, b) Argentinian soil dust, c) Snomax, d) Illite NX, and e) Moroccan desert dust, as a function of the d_{va} measured by ALABAMA (blue), ATOFMS (orange), LAAPTOF (green), PALMS (red), and miniSPLAT (black). Note that the uncertainty for super-micrometer particles is larger due to the low number concentration of these particles in the experiments. The DE curves in white and shaded area are based on SMPS and APS results, respectively. There were overlap results between SMPS and APS for the sizes around 700 nm to 1 μm d_{va}. In such an overlap range, we chose SMPS data as reference to calculate DE. Given different shape factors and particle densities, the conversions of d_m and d_{ca} to d_{va} were different for different particle types. Therefore, the end point of SMPS based result or shift point between white and shaded area varies from sample to sample. Noted that the DE of miniSPLAT is defined differently from the other SPMSs. The sized distribution derived DE (dashed black) and the hits only derived DE (solid black) for K-feldspar is shown to provide the upper and lower limits of miniSPLAT DE (see text for details).
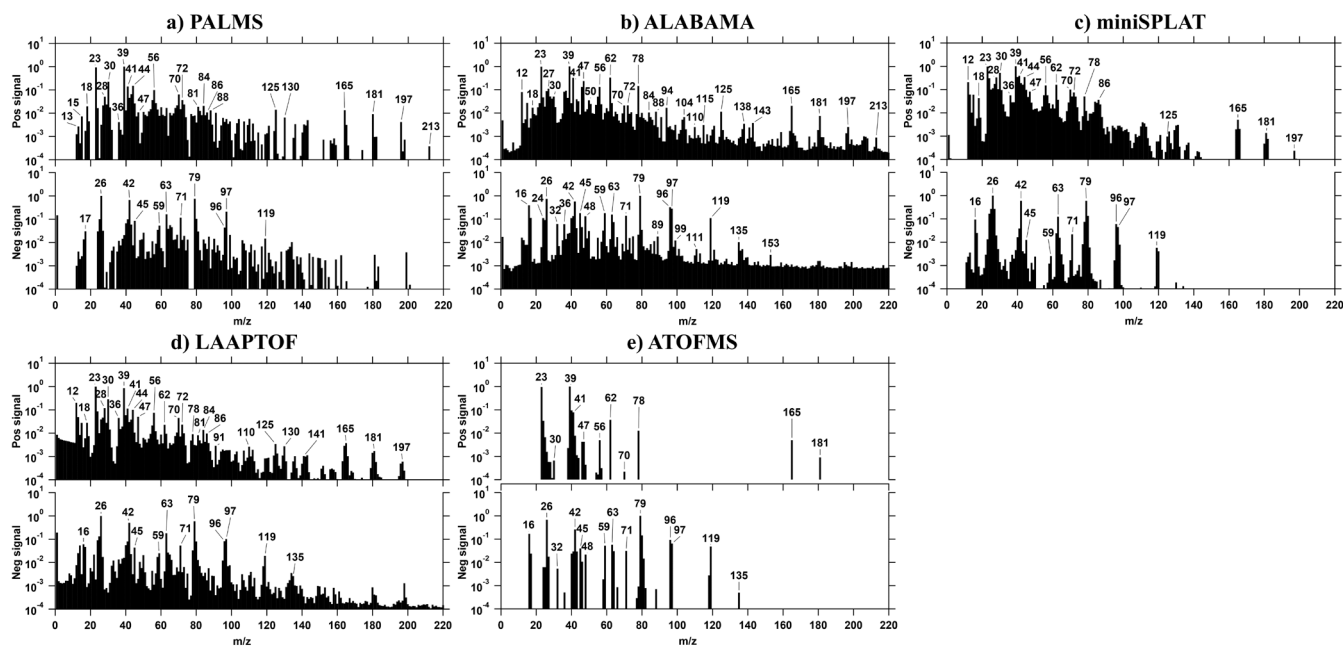
Figure 54: Normalized average mass spectra of Snomax, measured by a) PALMS, b) ALABAMA, c) miniSPLAT, d) LAAPTOF, and e) ATOFMS. The numbers of spectra averaged for each are 973 a), 1018 b), 2327 (c), 260 d), and 1071 e).
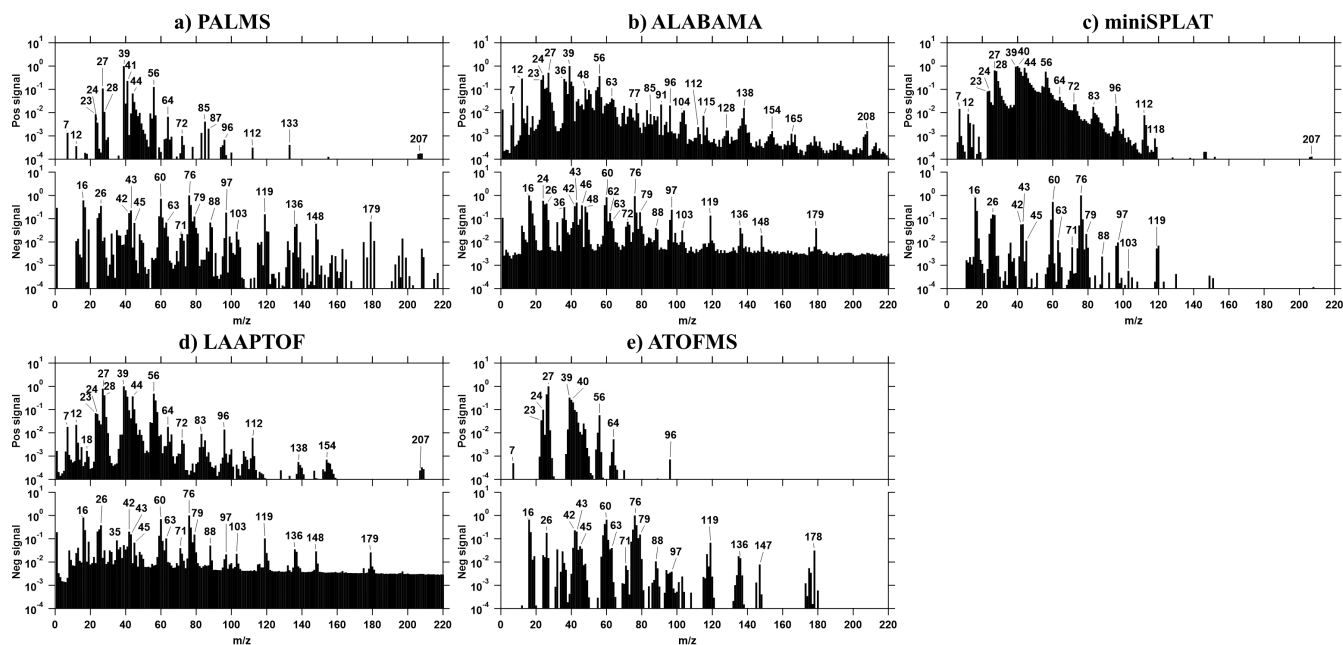
Figure 65: Normalized average mass spectra of Moroccan desert dust by a) PALMS, b) ALABAMA, c) miniSPLAT, d) LAAPTOF, and e) ATOFMS. The numbers of spectra averaged for each are 715 a), 353 b), 346 (c), 215 d), and 1447 e).

900
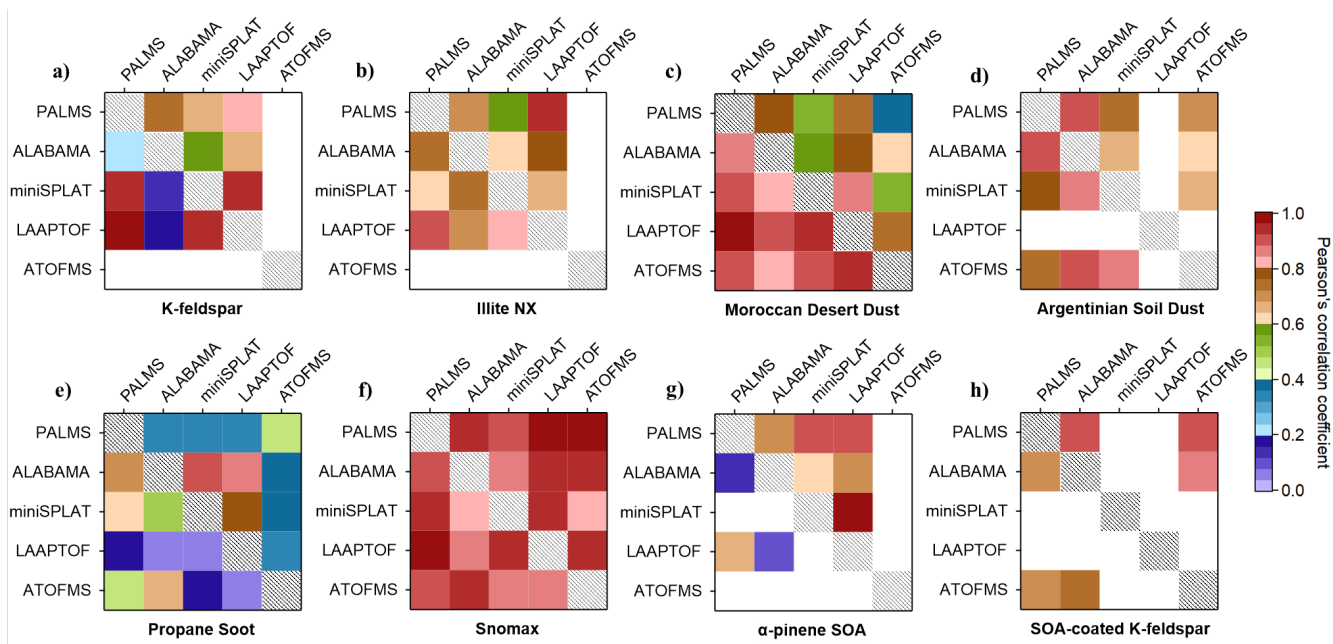
Figure 7̶6: Correlation plots of average spectra of the different particle samples a) K-feldspar, b) Illite NX, c) Moroccan desert dust, c) Argentinian soil dust, e) propane soot, f) Snomax, g) α-pinene SOA, and h) SOA-coated K-feldspar, analyzed by the five SPMSs. Within each diagram correlation results for positive spectra are upper right and negative spectra are bottom left. White cubes denote cases where no data is available.

905
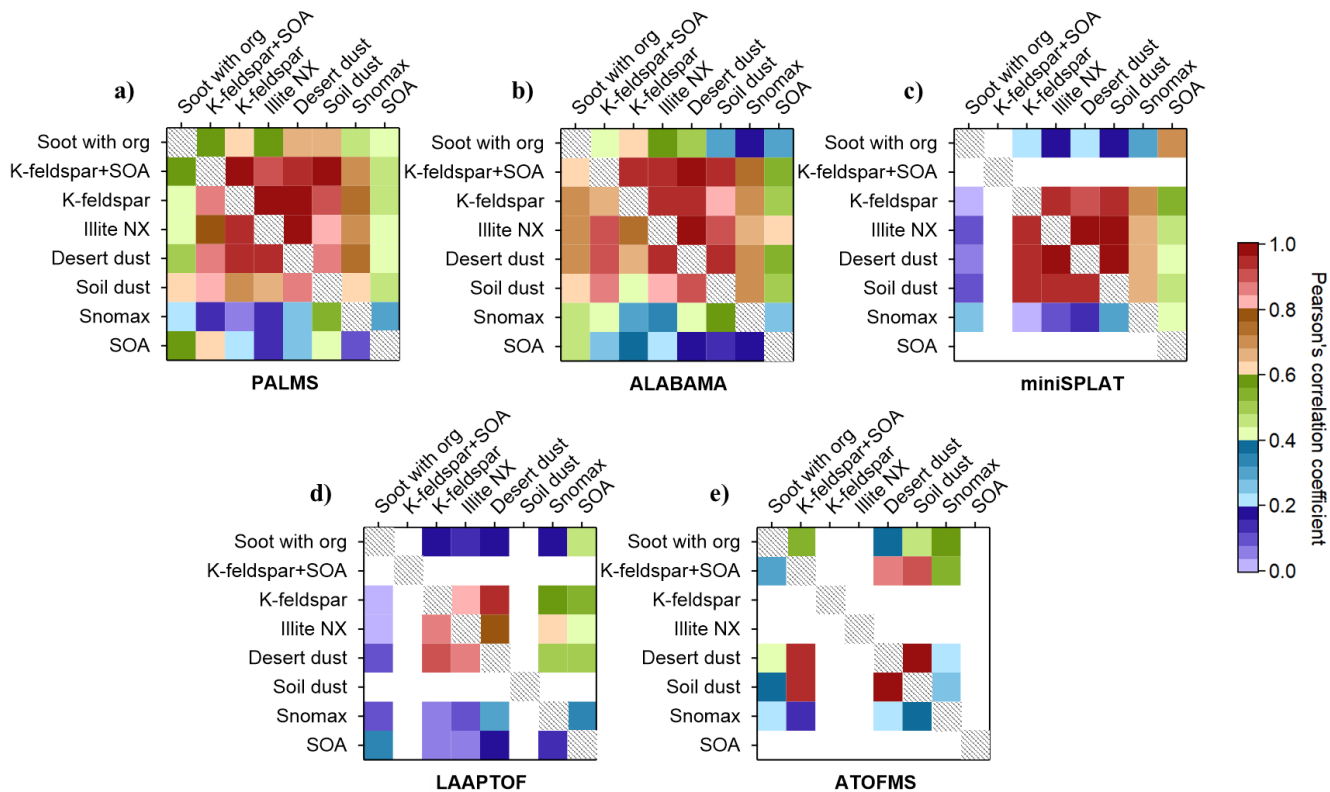
Figure 8̶7: Correlation plots of average spectra of different samples analyzed by a) PALMS, b) ALABAMA, c) miniSPLAT, d) LAAPTOF, and e) ATOFMS. Correlation results for positive spectra are upper right, while negative spectra are bottom left. Note that, the soot with organics and K-feldspar+SOA denote the propane soot and SOA-coated K-feldspar, respectively.
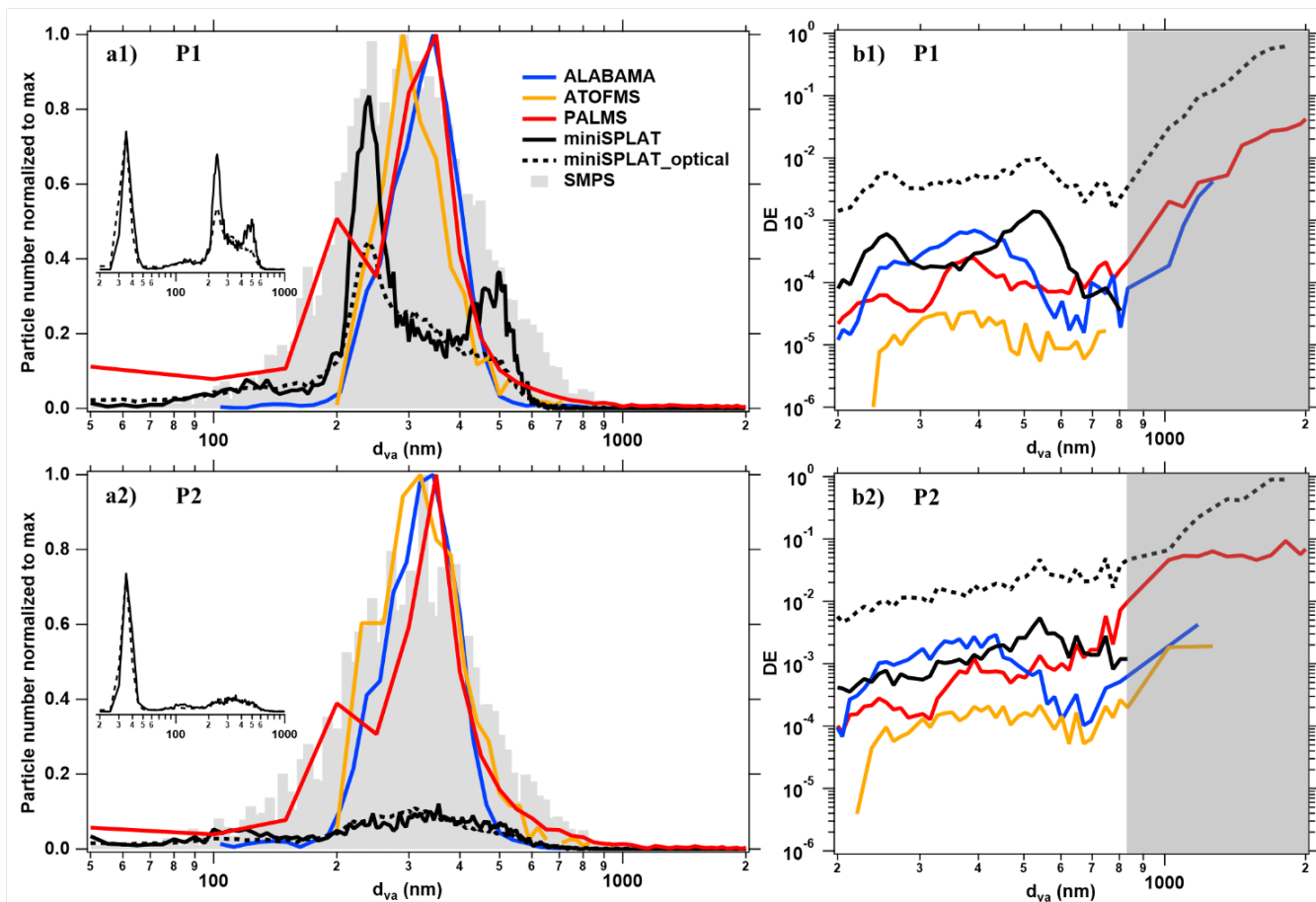
915

Figure 9̶8: Particle size distribution and DE of PALMS (red), ALABAMA (blue), ATOFMS (orange), and miniSPLAT (black) during two different time periods (P1 and P2) of the blind experiments. For miniSPLAT, the full-size ranges measured during P1 and P2 are inserted in a1) and a2), respectively (note that the smallest size mode appears large, due to the lognormal mode in the X-axis). Note that the dashed black curves represent the DE of the whole size distribution measured by miniSPLAT, while in the solid black

920 curve represent DE consistent with the other SPMSs (see text for details). d_m measured by SMPS (grey) was converted to d_{va} for comparison. The DE curves in the white and shaded areas are based on SMPS and APS results, respectively. f_m =1.13 and f_{ca}= 1.06, the number weighted values derived from α-SOA and Argentinian soil dust (particle number ratio of 2:3), were used in these experiments. Note most of the soot particles were below the detection limit of SPMSs, with the exception of miniSPLAT (see text for details).
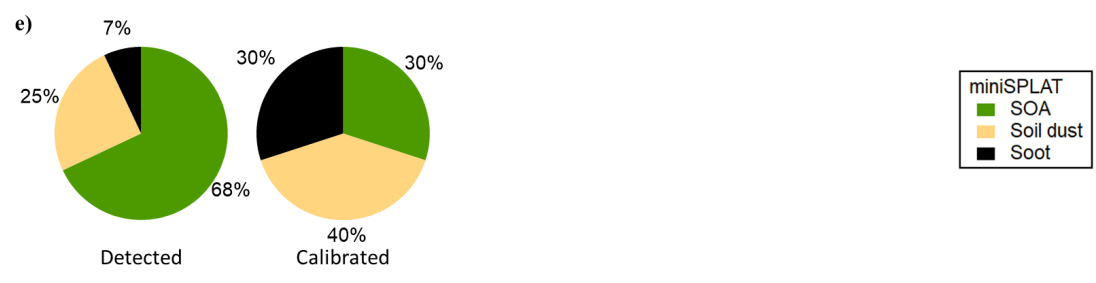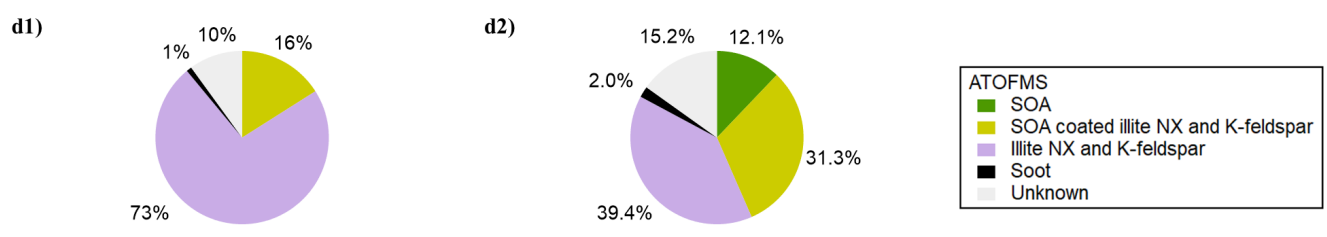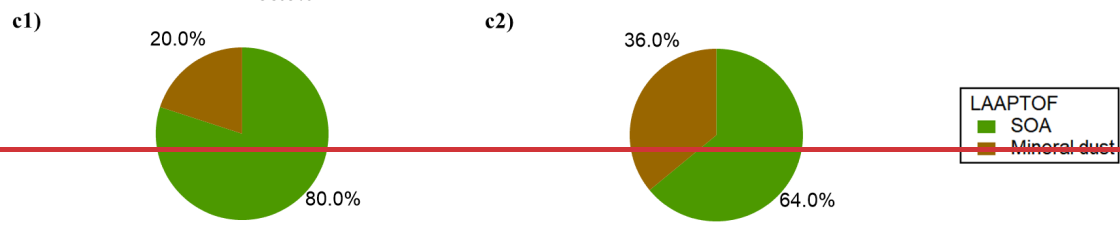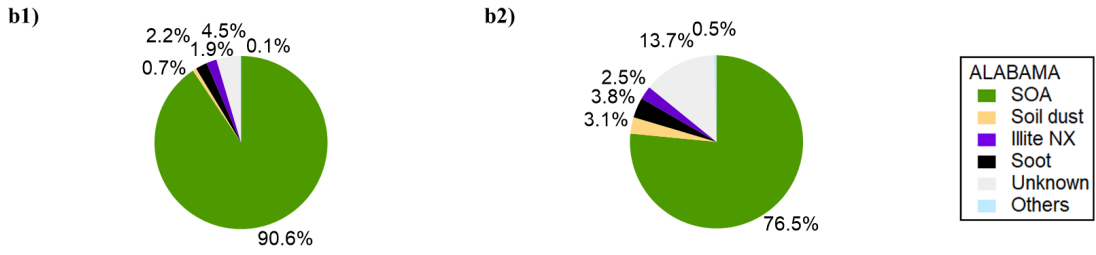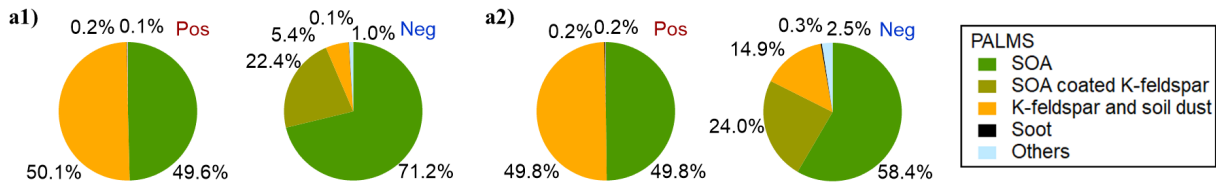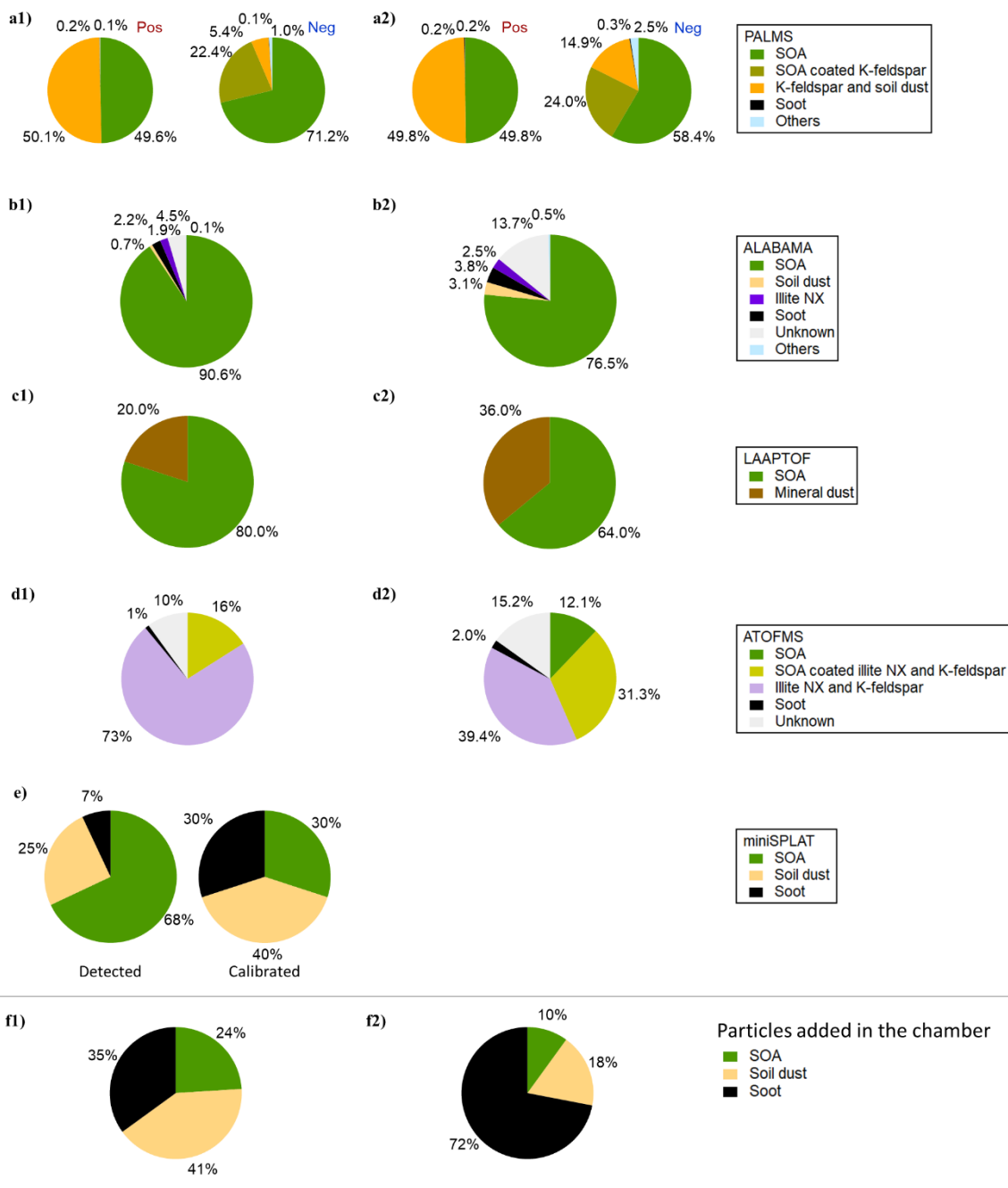
Figure ~~10~~9: Particle classes and their relative contributions for blind periods P1 and P2 for: a1-2) PALMS, b1-2) ALABAMA, c1-2) LAAPTOF, d1-2) ATOFMS and e) miniSPLAT (which only reported data in P1). f1-2) are the ~~same~~ pie charts as those in Fig. 1. added here for better comparison. The plots shown here are the data provided to the referees after experiments (i.e., before participants knew the composition of the blind experiment). Note the left pie chart for miniSPLAT represents acquired mass spectra, consistent with what is presented for the other SPMSs. The right pie chart, provided to the referees after experiments, represents calibrated data (see text for details). Particle clustering is shown for positive and negative spectra separately for the unipolar switchable PALMS instrument.